ELECTRICAL AND OPTICAL PROPERTIES OF AMORPHOUS MATERIALS

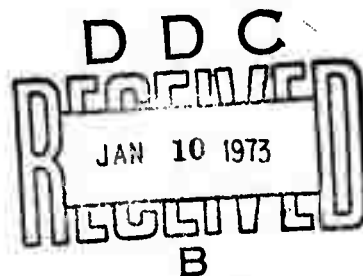Charles Wood

Northern Illinois University

FIFTH SEMI-ANNUAL TECHNICAL REPORT

December, 1972

ELECTRICAL and OPTICAL PROPERTIES OF AMORPHOUS MATERIALS*

by

A Solid-State Group of the Physics Department
Northern Illinois University
DeKalb, Illinois   60115

*Sponsored by
Advanced Research Projects Agency
ARPA Order No. 1562

The views and conclusions contained in this document are those
of the authors and should not be interpreted as necessarily
representing the official policies, either expressed or implied,
of the Advanced Research Projects Agency or the U.S. Government.

"Approved for public release; distribution unlimited."

GENERAL INFORMATION

ARPA Order Number   1562

Program Code Number   OD10

Name of Contractor   U.S. Army Research Office

Effective Date of Contract   June 1, 1972

Contract Expiration Date   May 31, 1973

Amount of Contract $39,000.00

Contract Number   DA-ARO-D-31-124-72-G115

Principal Investigator   Dr. Charles Wood
                                    (815) 753-1773

I

CONTENTS

SUMMARY

Despite the handicap of the lack of band structure calculations for Sb_2Se_3 we have developed an approach where, by comparison of the optical, x-ray photoemission, and U.V. photoemission spectra, we have been able to assign features of the spectra of amorphous and single crystal Sb_2Se_3 to originate from densities of states in the valence and/or conduction bands and to identify the nature of the transitions i.e. direct or indirect between regions. A model based on a chemical-bonding approach has been employed to explain the overall features of the spectra.

Our method of Kramers-Kronig analysis of optical data has stood-up well to the test of newly-developed sum-rules further strengthening our confidence in this technique.

Experimental research into the crystalline and amorphous Sb-Se system is nearing its final stages. Work is continuing on optical photo-emission and photoconductivity studies but, in the past six months, we have emphasized transport measurements, i.e., electrical conductivity and thermo-e.m.f., on single-crystals, quenched ingots, and amorphous films.

The elongated substrate technique for preparing a whole "phase-diagram" of amorphous films has been developed and has come to fruition. This has allowed the investigation of essentially the whole Sb-Se system in one fell swoop. We are now proceeding in the same manner with the Ge-Se and Ge-Te systems.

Photoconductivity measurements of Sb_2O_3 essentially corroborate the optical data. We do not plan to carry-on further with this material at this stage.

Mössbauer studies have been chiefly concerned with attempts to correlate isomer shifts and quadrupole splittings with electronic structure in amorphous solids both for our measurements and for literature data.

We anticipate phasing out work on the Sb-Se system early in the next six-month period and exploring the extremely interesting Ge-chalcogenide amorphous systems.

The appendices include a preprint of a paper summarizing the main features of our photoemission data on amorphous and crystalline Sb_2Se_3; a preprint describing our elongated substrate technique of preparation of thin amorphous films including its application to the Sb-Se system; a photoconductivity paper on crystalline and amorphous Sb_2O_3, and an abstract of a paper to be presented at the 8th Mössbauer Conference in New York in January 1973 reviewing Mössbauer studies on amorphous materials. In addition a report on our photoemission work on amorphous and crystalline Sb_2Se_3 was presented at the 5th Synchrotron Radiation Users Group Conference at the University of Wisconsin, November 1972.

I.   THEORETICAL RESEARCH

A. Model Densities of States for Crystalline and Amorphous Sb_2Se_3

With the rather large amount of experimental information presently available on the electronic structure of crystalline and amorphous Sb_2Se_3 it should now be possible to interpret this accumulated data in terms of model densities of states for the crystalline and amorphous materials. Particularly interesting is the possibility that the (rather small) differences in optical and other spectral properties between the two forms of the compound may be assigned to influences of the loss of long range order on the electronic structure or upon changes in matrix elements for optical transitions. Since the chemical bonding in the material is also reflected in the electronic structure such a study may have valuable spin-off in understanding the stereochemistry in V-VI compounds on condensation in amorphous form. (Although Sb_2Se_3 does not quench as amorphous from the melt it can be made amorphous by evaporation and is chemically representative of the V-VI compounds).

For the purpose of constructing model densities of states for Sb_2Se_3 in its two forms the experimental data of most direct interest are (1) (XPS), x-ray photoelectron spectroscopy, (2) optical reflectivity and optical functions e.g., $\varepsilon_2(\omega)$, derived therefrom, and (3) photoemission spectra. Results and their tentative interpretation for each of these spectroscopic methods were presented in the previous semi-annual report, and have either been published (1,2) or submitted for publication (3).

To outline our model approach we recall that XPS data provide us with
an (unnormalized) valence band density of states of resolution about 1eV
(1). We can normalize this data approximately using the sum rules from
the optical data (2). Photoemission results (3) locate absolutely struc-
tural features in both the occupied (valence) and unoccupied (conduction)
band densities of states. From these data we can construct a parametrized
conduction band density of states as well as refining the XPS valence
band structure. We then make use of the fact that the optical functions
may all be derived from the joint optical density of states (we assume
constant or slowly varying matrix elements). The quantity $\hbar^2\omega^2\varepsilon_2$ is pro-
portional to the joint density of states. Now if, indirect transitions
dominate the spectrum or if it is determined mainly by contributions from
flat bands through the bulk of the zone we may employ the formula (for
each crystalline orientation and the amorphous material, separately)

$$\hbar^2\omega^2\varepsilon_2(\omega) = C\int_{Eg}^{\infty} N_c(E)N_v(E - h\omega)dE$$

where N_c and N_E are unoccupied and occupied densities of states respec-
tively and C is a constant for each case. Certainly this should be satis-
factory for the amorphous material. Further it should describe the bulk
features of the optical response of the crystalline system since the
photoemission results indicate that much of the structure arises from
flat bands. Additional features which redistribute oscillator strength
will be related to (1) failure of the "indirect transition" formula, im-
plying that $\hbar^2\omega^2\varepsilon_2(\omega)$ should be found from the "direct" transition formula:

$$\hbar^2\omega^2\varepsilon_2 \sim |\underline{e}.\underline{M}_{vc}|^2 \Sigma_{\underline{k}} \delta(E_f(\underline{k}) - E_i(\underline{k}) - h)$$

or (2) anisotropy in $|\underline{e}.\underline{M}_{vc}|$ and thus different energy dependence in that

quantity, for different crystalline orientations.

B. New Sum Rules

Although we have rigorously tested our Kramers-Kronig analysis by demanding that several sum rules be obeyed (2) new sum-rules have been recently obtained by Altarelli et al (4). In particular, they have found the sum rule.

$$\int_0^\infty (Re\left[\hat{n}(\omega)\right] - 1)d\omega = 0$$

This rule is valuable as a critical test of a Kramers-Kronig analysis for a particular set of data. This is particularly true if the data extends to near saturation of $Re(\hat{n}(\omega))$, i.e., if it is converging toward 1.0. We have made this final test of our derived optical constants while proceeding with the program described above to assure the accuracy of the optical data to which we fit. Since the calculation extrapolates the data into the unmeasured region by fitting the data near the boundaries by classical dispersion formulae the sum rule above tests the validity of the extrapolation. The results suggest that the extrapolations used are quite good. For example, for the case of amorphous Sb_2Se_3 we computed the integral above by dividing it into three portions as follows:

$$I_1 = \int_0^{25}(n(\omega)-1)d\omega$$
$$I_2 = \int_{25}^{500}(n(\omega)-1)d\omega$$
$$I_3 = \int_{500}^\infty(n(\omega)-1)d\omega$$

where $\hat{n}(\omega) = n(\omega) + ik(\omega)$.

I_1 and I_2 are integrated numerically directly from the results of the Kramers-Krönig analysis and the extrapolation, respectively. I_3 is integrated analytically by employing the (accurate) approximation $n = 1 - \omega_p^2/\omega^2$. The results with estimated computational error are:

$$I_1 = 7.563 \pm .02$$
$$I_2 = -6.924 \pm .05$$
$$I_3 = -0.731 \pm .01$$

Thus, $I_1 + I_2 + I_3 = -.092 \pm .08$, which indicates that the extrapolations are compatible with the data and the inversion procedure.

II.   RESEARCH ON Sb_2Se_3

A. Spectroscopic Studies of Electron States of Crystalline and Amorphous Sb_2Se_3

1. Introduction

The work on the electronic structure of crystalline and amorphous Sb_2Se_3 is essentially complete. Within the limitations imposed by the absence of a band structure calculation a fairly complete picture of the electronic structure based upon a valence bonding model has been developed. Comparison of optical reflectivity (with Kramers-Kronig analysis), x-ray photoelectron spectroscopy, and photoemission (see Appendix A) has led to this model. Various aspects of this work are reported in three publications (1,2,3,) and for the future it is planned to summarize this with a more detailed model analysis in one comprehensive publication.

2. Reflectivity and Transmission Measurements

Detailed work on the optical absorption edge has been completed in the past six-months on both amorphous and crystalline Sb_2Se_3 as a function of temperature. The results show that the absorption edge in the crystal for both $\underline{E}||a$ and $\underline{E}||c$ begins with an indirect transition and then rapidly transforms into a direct allowed transition. The shift of the gap for the crystal to lower energies with increasing temperature has been reported (5) to be 7×10^{-4} eV/°C. For the amorphous phase the edge can be fitted to a $(\alpha h\nu)^{\frac{1}{2}}$ versus photon energy relationship over a large range of α's,

as shown before (6), i.e. the k-conservation selection rule is relaxed. The shift of absorption edge with temperature corresponds closely to the single crystal shift. This work will soon be ready for preparation for publication.

3. Photoemission

In the photoemission area, most of the effort was devoted to further analysis of the energy distribution curves (EDC's) for amorphous and crystalline Sb_2Se_3 in the photon energy range 7 to 20 eV, obtained using the UW Synchrotron storage ring. A preprint of a paper (submitted to Phys. Rev. Letters) which presents the main features, is attached as Appendix A. The main conclusions, as derived from the EDC's, are:

a. Splitting of the valence band into "bonding" and "weakly bonding" similar to the XPS data.

b. The "weakly bonding" band containing 12 electrons per Sb_2Se_3 molecule.

c. The existence of several flat E vs k bands in the upper 3 eV of the valence band, and in the upper conduction band (7 to 10 eV above the valence band maximum), much weaker in amorphous Sb_2Se_3.

d. The upper 3 eV of the "weakly bonding" band is very strongly affected by the phase transition. The resonance orbitals (either Se lone p-pairs or pivotal resonance bonds), characterised by very narrow E vs k bands in the crystal are strongly smeared out in amorphous Sb_2Se_3 as evidenced by the photoemission EDC's.

e. These resonance states are very strongly affected by the crystal field as evidenced by the strong dependence of matrix element oh $\vec{E}_0$ in the case of the crystal.

To conclude, the EDC's provide a set of data which allow further interpretation of the reflectance, and of the X-ray structure measurements. The new feature of our work is also the combination of the optical sum rules with the EDC's.

Future plans include measurements of cesiated Sb_2Se_3 to study the lower part of the conduction band, and measurements of EDC's during crystallization of amorphous Sb_2Se_3, as well as Sb_2Te_3 and Sb_2O_3.

B. Comparison of Photoconductivity and Resistivity Versus Temperature Studies

The variation of thermal activation energy with stoichiometric deviations around Sb_2Se_3 in single crystal and quenched polycrystals is being compared with photoconductivity threshold measurements on the same samples. It appears that considerable deviations from stoichiometry can occur depending on method of preparation of crystals and this accounts for conflicting reports in the literature of the value of the energy gap for Sb_2Se_3 (6).

The ac photoconductivity of the Sb_xSe_{1-x} samples was measured using the Baush & Lomb high intensity monochromator, and the Keithley 82 series lock-in amplifier. Gold contacts were carefully shielded from illumination to prevent any photovoltaic effects. The activation energy of the Sb_xSe_{1-x} was determined from the half-maximum of the normalized photoresponse using the Moss criterion. The results are presented in the following table, and

compared with the activation energy obtained from the resistivity measurements. Also the thermopower of the three polycrystalline samples (p-type) is presented.

SAMPLE	#1 Quenched Ingot 60.0% Se 40.0% Sb	#2 Quenched Ingot 62.5% Se 37.5% Sb	#3 Quenched Ingot 65.0% Se 35.0% Sb	#1 Single Crystal Sb_2Se_3	#2 Single Crystal Sb_2Se_3	#3 Single Crystal Sb_2Se_3
Eg (eV) ρ vs T	1.06	.97	.97	1.05	1.30	.90
Eg (eV) PHOTOCONDUCTIVITY	1.08	.97	1.10	1.07	1.12	1.10
Eg (eV) OPTICAL				1.07	1.10	1.08
SμV/$^\circ$c at 20°c	870	890	850			

C. Preparation and Characterization of Sb-Se Thin Films

The elongated substrate technique for preparing thin films of progressively varying composition has been fully developed and applied to the Sb-Se system. The films, extending from almost pure Sb to almost pure Se, have been characterized by optical and transport (resistivity and thermo emf) measurements as a function of composition. The data has been successfully analyzed using current theories applicable to amorphous semiconductors. A chemical bonding model has been employed to explain the variation of physical properties with composition. A full report is given in Appendix B. This method has proved to be exceedingly expeditious in exploring amorphous "phase-diagrams" and is currently being applied to other systems,

e.g., Ge-Se and Ge-Te.

D. Thermopower and Photothermopower

A system for measuring the thermopower (in dark or under illumination) down to $4°K$ has been constructed, and tested with satisfactory results using Sb_2Se_3 single crystals.

Photothermopower measurements are also in progress. In addition to the standard method with white light illumination (used primarily to decrease the sample's resistance), the spectral distribution and quenching of the photothermopower are also investigated. This method is promising in that it provides further information on the states within the band gap. A new method of "ac photothermopower", or "photomodulated" thermopower is being developed, which has at least 10^4 times higher signal to noise ratio due to the application of the synchronous detection technique.

III. RESEARCH ON Sb_2O_3

A. Photoconductivity

Photoconductivity measurements were performed on Sb_2O_3; for both crystalline modifications, the photoresponse is consistent with the optical absorption, with the impurity photoconductivity band in the case of cubic Sb_2O_3. In amorphous Sb_2O_3, no photoresponse was detected, due probably to much lower "internal photosensitivity" $\mu\tau$ (mobility times the lifetime). A preprint of this work is presented as Appendix C.

IV.   STRUCTURAL RESEARCH

A. Mossbauer Effect

A comprehensive review of the implications of Mossbauer studies upon
amorphous materials for the understanding of electronic structure, chemical
bonding and structure (7) and the glass-crystal transition (8) in materials
containing iron, antimony, or tin is in preparation for presentation at the
8th Mossbauer Conference in New York (January 28, 1973). Studies carried
out in this laboratory as well as others are presented and discussed. An
abstract of this review is attached as Appendix D.

Preceding page blank

REFERENCES

1. C. Wood, J.C. Shaffer, and W.G. Proctor, Phys. Rev. Ltrs., 29, 485 (1972).

2. J.C. Shaffer, B. Van Pelt, C. Wood, J. Freeouf, K, Murase, and J.W. Osmun, Phys. Stat. Sol. 54, (1972).

3. Z. Hurych, D. Buczek, C. Wood, G.J. Lapeyre, and A.D. Baer (submitted to Phys. Rev. Ltrs.).

4. M. Altarelli, D.L. Dexter, H.M. Nussenzweig, and D.Y. Smith (preprint, Phys. Rev. (in press)).

5. J. Black, E.M. Conwell, L. Seigle, and C.W. Spencer, J. Phys. Chem. Solids 2(3): 240 (1957).

6. C. Wood, Z. Hurych, and J.C. Shaffer, J. Non. Cryst. Sol. 8-10, 209 (1972).

7. S.L. Ruby. L. Gilbert, and C. Wood, Phys. Letters 37A, 453 (1971).

8. S.P. Taneja, A.E. Dwight, L. Gilbert, W. Harper, C.W. Kimball, and C. Wood, Phys. Chem. Glasses, 13, (1972).

FISCAL STATUS

	Amount Allocated	Amount Spent	Balance
Personnel	$ 30,500.00	$ 18,059.64	$ 12,440.36
Supplies, Expenses and Services	2,020.00	3,147.59	- 1,127.59
Travel	900.00	360.61	539.39

TOTAL BALANCE $ 11,852.16

APPENDIX A

Analytical Subject Index: "Solids"

<div align="center">

Photoemission Spectra of
Crystalline and Amorphous Sb_2Se_3

</div>

<div align="center">

Z. Hurych, D. Buczek and C. Wood[†]
Physics Department
Northern Illinois University
DeKalb, Illinois 60115

and

G.J. Lapeyre and A.D. Baer[††]
Physics Department
Montana State University
Bozeman, Montana 59715

</div>

Abstract

The photoemission energy distribution curves (EDC's) of crystal-line and amorphous Sb_2Se_3 were measured in the photon energy range $h\nu = 7$ to 20 eV using polarized radiation from a synchrotron storage ring. The EDC's show several regions of high density of states in both the valence and conduction bands, with the structure strongly smeared-out in amorphous Sb_2Se_3. The region of the upper 2 eV of the valence band, containing six electrons per Sb_2Se_3 molecule, is clearly separated from the remaining part of EDC's in crystalline Sb_2Se_3. The optical transitions in crystalline Sb_2Se_3 are direct, with matrix elements strongly dependent on the orientation of the electrical vector of the polarized radiation. No evidence was found to indicate that the wave-vector $\vec{k}$ provides a significant quantum number in amorphous Sb_2Se_3.

The vacuum UV photoemission spectra of amorphous and crystalline Sb_2Se_3 were measured over the photon energy range 7 to 20 eV using the University of Wisconsin 240 MeV synchrotron storage ring. The radiation incident onto the sample was naturally polarized ~80% with the electrical vector E_0 in the medial plane of the storage ring. A double-pass cylindrical electrostatic mirror (1) with a spiraltron was used as an electron energy analyzer having a constant resolution of ~0.2 eV. Orthorhombic Sb_2Se_3 single crystals (space group D_{2h}^{16}), grown in a zone refiner, (2), were cleaved in situ in a vacuum background of the ~10^{-10} torr. The natural cleavage plane (010) produced excellent mirror-like surfaces which allowed the measurement of the photoemission energy distribution curves (EDC's) for $E_0 || a$ and $E_0 || c$. Amorphous Sb_2Se_3 films of thickness 200 to 500 Å were evaporated in situ from an electron-beam gun by a method developed earlier (3). X-ray diffraction measurements after the photoemission experiment confirmed that the films were amorphous. The complete experimental details and results are beyond the scope of this letter and will be published separately. Here several typical EDC's of Sb_2Se_3 are presented and their relation to the electron energy states is discussed.

The main features of the EDC's for crystalline Sb_2Se_3 are four peaks A, B, C, and D of constant and well-defined energy of the initial states, (fig. 1). The intensity of each of these four peaks is strongly varying with the photon energy which indicate that they correspond to direct (i.e., $\vec{k}$ conserving) optical transitions. A weak shoulder S on the leading edge was also observed. Since the two peaks A and B are present over the entire photon energy range with constant energy of initial states, we associate

them with the regions of high density of states arising from narrow bands or from flat E vs. k portions of the valence band. A valley V, located 2 eV below the valence band maximum is one of the most prominent features of the EDC's for both orientations of E_0. A weakly resolved onset of a deeper-lying valence band at ~ 6 eV below the valence band maximum, superimposed on the background of scattered electrons and on the conduction band structure, is observed as an inflection (point G) in the EDC's for $h\nu \geq 17$ eV. The existence of this band has been confirmed by X-ray photoemission spectra (4). The lower energy ranges of the EDC's indicate four peaks P_1 to P_4 of intensity and shape strongly varying with $h\nu$, which indicate direct optical transitions. Since these peaks are present over the entire photon energy region with constant energy of final states, we associate them with the regions of high density of states in the conduction band. These states are coupled in direct optical transitions with the regions of high density of states in the upper part of the valence band, thus giving rise to very sharp peaks in the EDC's (e.g., the pair D and P_3 for $E_0 || a$). An important feature of the EDC's is the dependence of the relative intensity of the peaks A,B,C, and D on the orientation of E_0 (fig. 2). This dependence of the energy distribution of the joint density of states (JDOS) on E_0, which is not observable in the JDOS derived from the reflectance or $(\omega^2 \epsilon_2)$ spectrum, (4), (5), is attributed to the effect of the crystal field. The matrix elements for the optical transitions now include E_0 in addition to $\vec{k}$ and $\hbar\omega$.

According to the sum rules (5) the upper 2 eV of the valence band contains 6 electrons per Sb_2Se_3 molecule. These electrons can be associated with the 6 weakest (i.e. longest) bonds between the crystal layers in the Sb_2Se_3 molecule (6) which arise either from resonating p-bonds (7) (the Sb coordination is 7 and the Se coordination is 4 and 5) or from the three

pairs of "non-bonding" Se p-orbitals (lone-pairs) (8), (9). (The bond number of these weakest bonds between the crystal layers is $\sim$0.01 according to (6).) The crystal symmetry and field determine the direction of these bonds and their energy levels by minimizing the total crystal energy. From the sum rules (5) another 6 valence electrons per molecule are locate' between the valley V and point G. These states we attribute to resonant p-bonds of intermediate strength, forming the crystal layers from infinitely long Sb-Se chains. The deeper valence band starting at $\sim$6 eV below the valence band maximum (point G in the EDC's) is attributed to σ- bonding orbitals, arising from the strongest Sb-Se bonds within the chains. This band is of sp character, with the s states arising primarily from Sb4s. The strong coupling of the upper p-type part of the valence band with the high densities of states in the upper conduction band suggest the d-character of the latter states.

In amorphous Sb_2Se_3 (fig. 2) all peaks A,B,C, and D disappear, and a broad peak, located approximately half-way between A and B is observed. This broad peak (at $\sim$1.2 eV below the valence band maximum) of intensity and shape rather constant with respect to hv suggests that the optical transitions are non-direct, i.e., no evidence is found that the k conservation is an important selection rule. There appear two very weak conduction band structures P and P' located at $\sim$7 and 8 eV above the valence band maximum. As with Se and Te (10) the long range disorder has the effect of smearing the upper conduction band structure rather than affecting the sharpness of the leading edge of EDC's. No band tailing is observed within the experimental resolution, in agreement with previous optical and photoconductivity data (3) (11). The weaker conduction band structure

allows for much better resolution of the onset of the bonding band (point G) in amorphous than in crystalline Sb_2Se_3. The separation of the upper part of the valence band by the valley V is much weaker in amorphous Sb_2Se_3 yet still noticable. The weaker bonds, responsible formerly for holding the crystal layers together, are now randomly oriented in space, and their energy levels are determined locally by the random potential fluctuations, which result in a lack of the resonance character of these bonds.

REFERENCES

1. G.J. Lapeyre, A.D. Baer, P.L. Gobby, and C.F. Badgley, to be published and V.V. Zashkvara, M.I. Korunskii, and O.S. Kosmachev, Soviet Physics -- Technical Physics 11, No. 1, July (1966).

2. C. Wood, B. Van Pelt, and E. Hyland, Rev. Sci. Instr., 43, 9, 1374 (1972).

3. R. Mueller and C. Wood, J. Noncryst. Solids 7, (1972) 301.

4. C. Wood, J.C. Shaffer and W.G. Proctor, Phys. Rev. Letters 29, 8, 485 (1972).

5. J.C. Shaffer, B. Van Pelt, C. Wood, J. Freeouf, K. Murase and J.W. Osmun, phys. stat. solidi (in press).

6. N.W. Tideswell, F.H. Kruse and J.C. McCullough, Aeta Cryst. 10, 99 (1957).

7. E. Mooser and W.B. Pearson, J. Phys. Chem. Solids 7, 65 (1958).

8. E. Mooser and W.B. Pearson, Progress in Semiconductors 5, 104 (1960).

9. M. Kastner, Phys. Rev. Lett. 28, 6, 355 (1972).

10. L.D. Laude and B. Fitton, J. Noncryst. Solids 8-10, (1972), 971.

11. Z. Hurych, C. Wang, R. Mueller and C. Wood, J. Noncryst. Solids, 11, (1972) 153.

Captions to figures

Fig. 1. EDC's for $E_0||a$ (unnormalized). The insert shows the energy
position of the structures P_1 to P_4 in the conduction band as
determined with respect to the valence band maximum.

Fig. 2. Comparison of EDC's (unnormalized) for $E_0||a$, $E_0||c$ and for
amorphous Sb_2Se_3.
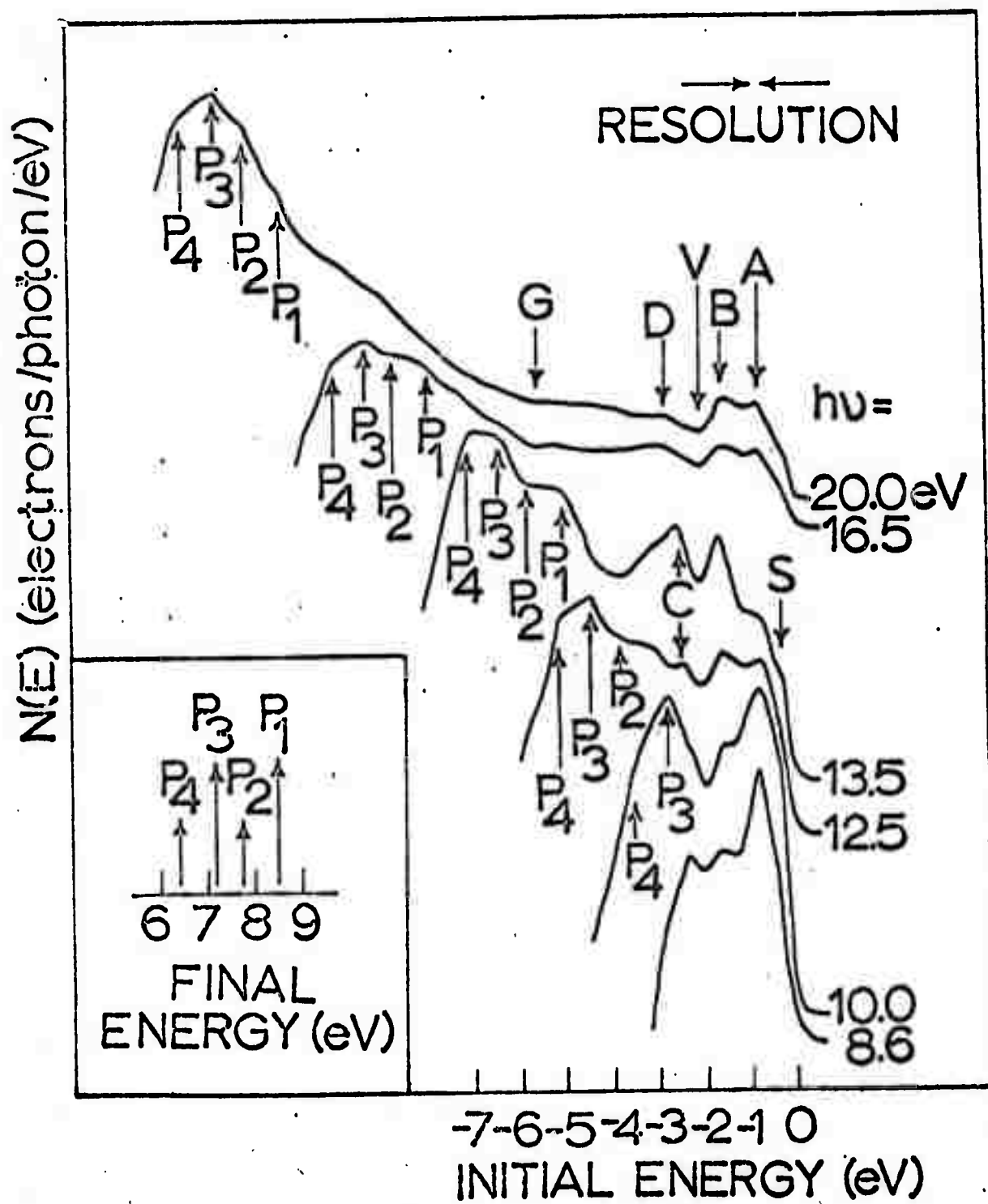
Captions to figures

Fig. 1. EDC's for $E_0||a$ (unnormalized). The insert shows the energy position of the structures P_1 to P_4 in the conduction band as determined with respect to the valence band maximum.
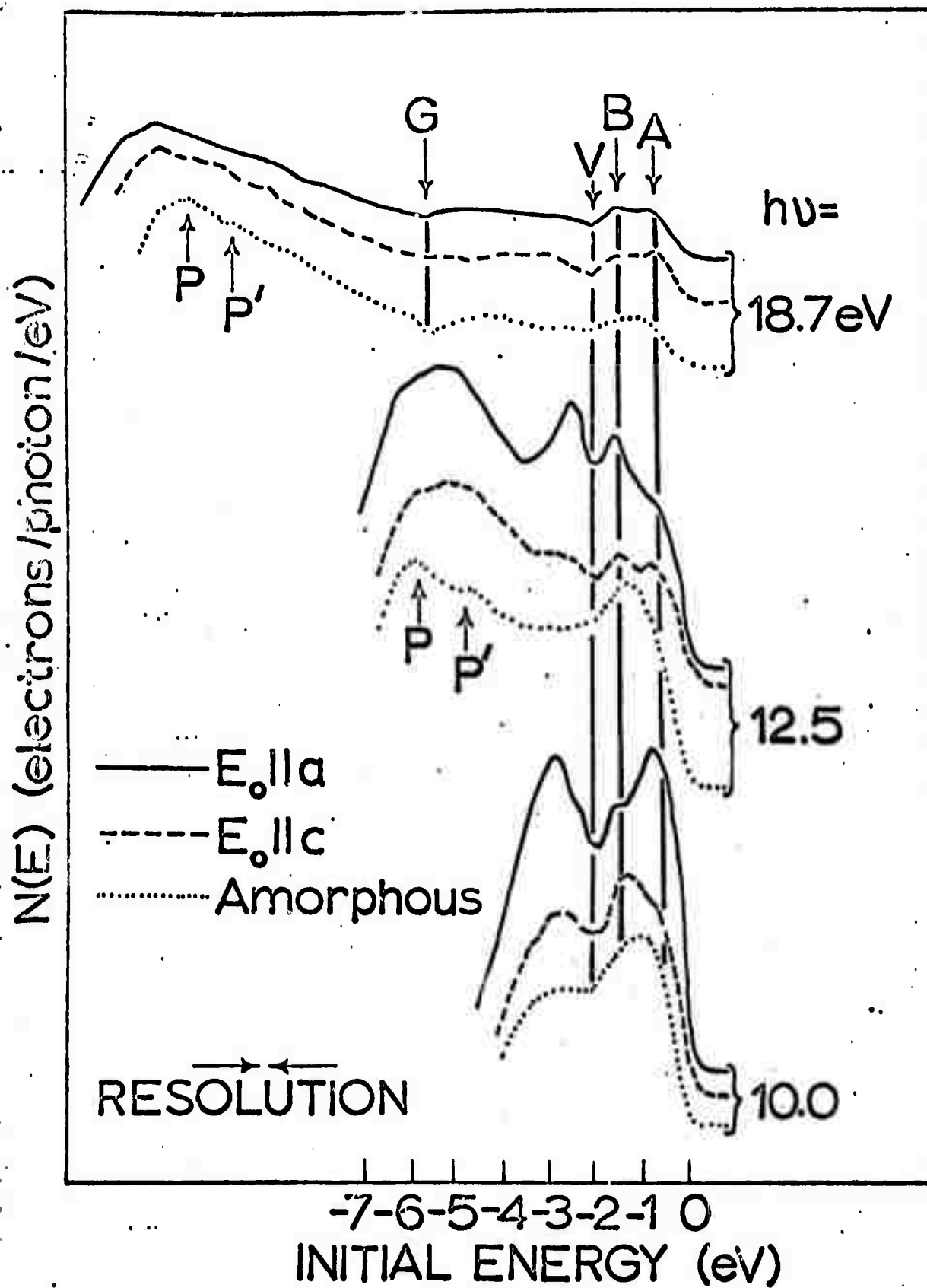
Fig. 2. Comparison of EDC's (unnormalized) for $E_0||a$, $E_0||c$ and for amorphous Sb_2Se_3.

29

APPENDIX B

THE AMORPHOUS Sb-Se SYSTEM*

C. Wood, R. Mueller and L.R. Gilbert

Physics Department
Northern Illinois University
DeKalb, Illinois 60115

Essentially the complete compositional range of the amorphous Sb-Se system has been prepared in thin-film form by a simple evaporation technique. Optical and transport properties have been measured as a function of composition.

1. Introduction

As pointed out in a previous paper[1]) considerable care is required in the preparation of amorphous materials by vacuum evaporation if a given composition is desired and, further, that physical properties, e.g. the optical energy gap, change appreciably as a function of composition. It is, therefore, of interest to investigate amorphous systems as a function of a wide range of known compositions and to construct a type of "phase-diagram". This can be a very laborious procedure by conventional methods and the purpose of this paper is to describe a method whereby such an investigation is facilitated and to apply this method to a particular amorphous system, namely, Sb-Se. The basic technique has been employed in the past to prepare crystalline films[2,3]) and composites[4])

but not, to our knowledge, to prepare amorphous films, i.e., its most appropriate use, where equilibrium phase diagrams are inapplicable and phase segregation is absent.

2. Experimental Apparatus

The apparatus is very similar in design to that described earlier[1]). Sb and Se are coevaporated from two Airco-Temescal electron beam (EB) guns whose relative rates of evaporation are controlled by two Sloan Omni IIA rate controllers[†]. However, the major difference between systems is that in this instance the EB guns are widely separated (diammetrically opposed) in the bell-jar and the substrate holder is ∿14 in. long, i.e., nearly equal in length to the diameter of the bell-jar (fig. 1). Thus a total of about 28 ½"X½" square fused-quartz substrates can be accomodated in a holder. The juxtaposition of one end of the substrate holder to one crucible and its remoteness from the other crucible ensures the formation of a strong composition gradient along the length of the holder; the actual value of the gradient and the film thickness depends on the density of Sb and Se, and on the height of the holder above the crucibles.

Our present system incorporates two such holders situated at different heights above the crucibles, clamped on to copper tubing cooled by liquid N_2. Hence, for a given ratio of evaporation rates from the two EB guns a broad sampling of compositions in thick films is obtained in the lower rack and a smaller compositional gradient about

---

[†]The operation of these controllers has been greatly improved by the redesign of the quartz crystal oscillator by Dr. D.E. Newell of the Industry and Technology Department, N.I.U.

the composition ratio of interest is obtained in thin films from the upper rack. Furthermore, the substrates can be held at temperatures between liquid N_2 and room-temperature.

3. Film Preparation

In this experiment the evaporations were carried out in a pressure of $\sim 10^{-7}$ mm Hg, or lower, and the ratio of evaporation rates for Sb:Se was chosen to be 1.0, thus Sb_2Se_3 occurred near the center of the substrate holder. The substrates were held at room-temperature throughout the evaporation. The compositions of selected films were determined by electron micro-probe analysis and are plotted in fig. 2.

A theoretical plot of film thickness (t) and composition (f), where f is the at% Se at point y, for the lower and upper substrate racks is also shown in fig. 2. A best fit to the experimental thickness data was obtained assuming an Sb:Se rate ratio ($W_{Sb}:W_{Se}$) of 0.7 instead of 1.0. These curves were plotted using the equations[5]:

$$t_{SbSe} = t_{oSb}\left[1+(\frac{y}{h})^2\right]^{-2} + t_{oSe}\left|1+(\frac{d-y}{h})^2\right|^{-2} \qquad (1)$$

$$f_{Se} = \left|1 + \frac{W_{Se}A_{Se}}{W_{Sb}A_{Sb}}\left(1+\frac{d^2-2dy}{h^2+y^2}\right)^2\right|^{-1} \qquad (2)$$

where t_{oSe}, t_{oSb} are the thicknesses directly above the respective sources; A_{Se}, A_{Sb} are the atomic weights of selenium and antimony; d is the separation of the sources; and h is the height of the rack. For this system, d equals 12.3 inches, h_{lower} equals 7.0 inches, and

h_{upper} equals 17.1 inches. Equations 1 and 2 include the assumption of a cosine distribution from each diameter source. At low evaporation rates, $\sim$1 to $1\frac{1}{2}$ Å/sec such as used in this experiment, this appears to be a reasonable assumption. However, Smith[6]) has shown that at high rates of evaporation from EB guns a virtual source exists and, therefore the source position and evaporation distribution are rate dependent.

Although both elements can be prepared in the amorphous form, amorphous Sb is stable only at low temperatures for thick films ($\sim$ microns) or for very thin films ($\sim 10^2$ Å) at room-temperature[7,8]). X-ray diffraction measurements showed that all except the extremely Sb-rich films were amorphous in the present experiment. The demarcation is shown in fig. 2. One film at this boundary appeared to be amorphous initially but crystallized on standing for a period of approximately one week. An indication of this transformation was first noticed optically by the initial appearance of infra-red optical transmission (and transmission interference fringes) and their later disappearance. The transformation was verified by X-ray diffraction.

4. Optical Measurements

In order to survey the optical properties of the films as a function of composition every alternate substrate in the sequence in the holder was selected for measurement. Because of the compositional variation across the substrate only a 1 mm wide strip of the center section, perpendicular to the composition gradient, was measured.

A Cary 14 R spectrophotometer with a Strong[9] reflectance attachment, was used to make optical transmittance (T) and reflectance (R) measurements. Since the films were deposited on fused-quartz substrates true R's and T's for the films were obtained from observed values R_{obs} and T_{obs} by using the equations[10,11], without a substrate in the reference beam:

$$T = \frac{T_{obs} \ (1-R_f' \ R_s')}{(1-R_s')} \tag{3}$$

$$R = \frac{R_{obs} - T_f^2 \ R_s'}{(1 - R_f' \ R_s')} \tag{4}$$

where R_f' the reflectance at the substrate-film interface was assumed to be $\simeq R_{obs}$, $R_s' = (1-n_s)^2 (1+n_s)^{-2}$ and the refractive index of the substrate $n_s = 1.43$.

The absorption coefficient (α) was calculated by computer programming the third-degree equation obtained by eliminating the front surface reflectivity, r, from the equations:

$$T = \frac{(1 - r)^2 \ e^{-\alpha t}}{1 - r^2 \ e^{-2\alpha t}} \tag{5}$$

$$R = r(1 + Te^{-\alpha t}) \tag{6}$$

i.e.

$$(e^{-\alpha t})^3 + \left[\left(\frac{1-R}{T}\right)^2 - 1 + \frac{1}{T^2}\right] T(e^{-\alpha t})^2 + \left[\left(\frac{1-R}{T}\right)^2 - 2\right]e^{-\alpha t} - \frac{1}{T} = 0 \tag{7}$$

These equations are valid only if the multiple-reflected rays are incoherent; and were applied only in the range where interference fringes were not observed. The short wave-length limit of the measured spectral range was set by the automatic slit-width of the Cary 14 R spectrophotometer reaching the fully-open position. Sample thicknesses, t, were determined by multiple interference of reflected light using a microscope fitted with a Watson interference objective. The refractive and absorption indices, n and k, were calculated from the equations:

$$\alpha = \frac{4\pi k}{\lambda} \, , \quad r = \frac{(n-1)^2 + k^2}{(n+1)^2 + k^2} \tag{8}$$

The absorption edges were found to obey the relation for non-direct transitions[12,13]

$$\alpha h\nu = B(h\nu - E_g)^2 \tag{9}$$

showing conservation of energy but not crystal momentum. If the intercepts of the extrapolated curves in fig. 3 are taken as the values of the optical energy gap (E_g) then one finds a tremendous variation in E_g from ~ 1.9 eV to ~ 0.4 eV on increasing the Sb:Se ratio. Corresponding values for B ranged from 10^6 to 2×10^5 cm^{-1}eV^{-1} (table 1).

The real part of the dielectric constant at high and low frequencies was obtained from the expression[14] from classical dispersion theory:

$$n^2 - k^2 = 1 + \frac{Ne^2}{m\varepsilon_o} \frac{\omega_o^2 - \omega^2}{(\omega_o^2 - \omega^2)^2 + \omega^2 g^2} \tag{10}$$

In the limiting case, where $n^2 \gg k^2$,

$$n^2 - 1 = \frac{Nef}{m\varepsilon_o} \frac{1}{(\omega_o^2 - \omega^2)} \tag{11}$$

and, further, where $\omega \rightarrow o$,

$$n^2 - 1 = \frac{Nef}{m\epsilon_o\omega_o{}^2} \qquad (12)$$

These experimental limiting cases are plotting for four representative films in fig. 4 as n^2 versus λ^2. The high frequency values of n were obtained from the cubic equation (7) in the region of non-interference, and the low frequency values, where k is small, were obtained from the positions of the maxima and minima in the interference region using the expressions:

$$2nd = m\lambda \ , \ m = \lambda_2/(\lambda_1 - \lambda_2) \qquad (13)$$

Extrapolations of the curves in fig. 4 to $\omega \rightarrow \infty$ and $\omega \rightarrow o$ yield values for the high frequency (ϵ_∞) and low frequency (ϵ_o) dielectric constants, respectively (table 2). The high frequency values are not very reliable because of the limited range of experimental values of n. As can be seen from fig. 4, a considerable error is introduced in the high frequency region if the n values determined from interference fringes are used for the extrapolation, as employed by Chandhari et. al[15]). This is further illustrated by the plot in fig. 4 of theoretical values of n, determined from equation 10 for $\omega_o = 3.0 \times 10^{15}$ sec^{-1} and $g = 1.5 \times 10^{14}$ sec^{-1}. Using the same values of n and k in Abèles equations[16]) interference fringes were generated and the values of n determined from the positions of the maxima and minima (eqn. 13) were plotted. The two curves are seen to diverge considerably at high frequencies as observed experimentally.

One cannot determine the free-carrier relaxation time and, hence, the charge carrier mobility, from the intersection of these two regions,

as suggested by Chandhari et. al.[15]). For high-resistivity materials, with very low free-carrier concentrations, such as discussed here and in ref. 15, the dispersion of the refractive index is due to an absorption band, not free-carriers as they supposed. The lack of absorption at long-wavelengths is confirmation that we are not dealing with dispersion due to free charge carriers in either the high or low optical frequency range.

5. Conductivity Measurements

Alternating in the holder with the substrates for optical measurements were substrates which were electroded for conductivity measurements. The electrodes consisted of 4 strips of baked-on liquid-bright platinum. After film deposition these substrates were clamped to a copper-block inside a copper radiation-shield attached to the cold-finger of an Air-Products Cryotip Dewar. Contact was made to the platinum by phosphor-bronze strips.

Up to 10^{13} ohms the resistances were measured by passing a known d.c. current through the outer two electrodes and, with a Keithley 604 Differential Electrometer (imput impedence 10^{14} ohms), measuring the voltage drop across the inner two electrodes spaced 2mm apart. Any potential barrier effects at contacts were thus avoided. Above 10^{13} ohms the resistances were determined from the current flowing with 500 volts applied across two electrodes. In films where the resistance variation with temperature required both 2- and 4-probe measurements $\ln \sigma$ versus $1/T$ curves coincided showing that contact potential barriers could be ignored. Teflon insulation was used throughout. The apparatus was calibrated with a series of standard resistances of up to 10^{13} ohms. The temperature of the film was measured by attaching a calibrated chromel-

constantan thermocouple to the film side of the substrate. The resistance was monitored both in the cooling and warming cycle. If sufficient time was allowed to come to equilibrium these curves coincided. The warming cycle had the slowest rate of change and generally was used for analysis. No hysteresis was observed between repeated cycles.

The results of these measurements are plotted in fig. 5. The activation energies were determined from a least-squares fit to the equation:

$$\sigma_0 \exp\left(-\frac{\Delta E}{kT}\right) \tag{14}$$

For conduction in extended states ΔE represents the energy difference between the Fermi-energy (E_F) and the majority carrier band edge (e.g. the valence band edge, E_v). For intrinsic conduction the Fermi-level is close to the center of the forbidden band and consequently $\Delta E = \frac{1}{2}E_g(0)$[17] i.e. the band gap at absolute zero temperature. If we assume ΔE to be a linear function of temperature

$$\Delta E = \Delta E_0 - \gamma T \tag{15}$$

then the value of ΔE obtained from the plots in fig. 5 is the extrapolated value (ΔE_0) to $T = 0°K$ and not the actual value of ΔE at $T = 0$[12,18].

The pre-exponential term, σ_0, includes the charge carrier mobility and density of states and can be shown to be closely invariant with respect to temperature for both conventional acoustic-mode lattice scattering in crystals and diffusive-type mobility[12,19] developed for disordered materials. Generally, σ_0 is not strongly temperature dependent compared to the exponential term in equation 14 and is expected to lie in the range 10^2 to 10^3 ohm^{-1} cm^{-1} [12].

If the charge carriers are excited into localized states at the band edges then $\Delta E = E_F - E_B + \Delta W_1$, where ΔW_1 is the activation energy for hopping conduction and the localized states occupy the energy range $E_B - E_V$. Here, σ_0 is expected to be $\sim 10^{-2}$ to 10 $ohm^{-1}cm^{-1}$ [12]). A straight line can be obtained on a $\ln\sigma$ versus $1/T$ plot if the mobility does not vary rapidly between E_B and E_V.

If hopping conduction occurs between localized states near the Fermi-energy then $\Delta E = \Delta W_2 \sim \frac{1}{2}$ width of the defect band. Again, a straight line $\ln\sigma$ versus $1/T$ plot can be obtained, with $\sigma_0 \lesssim 10^{-2}$ $ohm^{-1}cm^{-1}$, if hopping is between nearest neighbors. Otherwise,

$$\ln\sigma = A - B' T^{-\frac{1}{4}} \tag{16}$$

It is seen in fig. 5 that all but the extremely Sb-rich films yield a straight line on the $\ln\sigma$ versus $1/T$ plot. Values of $\sigma_0 \exp\left(\frac{\gamma}{k}\right)$, obtained by extrapolating the curves to $1/T = 0$ were found to be $\sim 10^3$ ohm^{-1} cm^{-1} on the Sb-rich side of Sb_2Se_3 and then to progressively decrease to ~ 10 ohm^{-1} cm^{-1} with increasing Se content (c.f. fig. 8). The extreme Se-rich films could not be measured in the present apparatus because of their very high resistance ($>10^{14}$ ohms). The extreme Sb-rich films were crystalline and showed metallic conductivity. The low temperature region of the film lying just on the amorphous side of the phase boundary, showed some curvature which could be fitted to the form of equation 16. However, an estimate of the density of states from $B' = 2[\alpha^3/kN(E_F)]^{\frac{1}{4}}$ yielded an unrealistic value of $N(E_F) \sim 10^{42}$ and so cannot be interpreted straightforwardly in terms of the Mott model. Annealing to produce an acceptable density of states value [20]) could not be employed here because of the propensity to crystallization.

6. Thermoelectric Measurements

The Seebeck coefficient (S) was measured on a number of the films used for resistivity measurements in an attempt to determine the position of the Fermi-level.

Several choices of expressions for Seebeck coefficient are available for amorphous semiconductors[12]. If the current is carried primarily by electrons (or holes) in the vicinity of the Fermi-energy (E_F) then:

$$S = \pm \frac{\pi^2}{3} \frac{k^2 T}{e} \left[\frac{d(\ln\sigma)}{dE} \right]_{E=E_F} \tag{17}$$

An equation of this general form is applicable to hopping conductivity and, for example, to a half-filled impurity or defect band.

For a one-carrier non-degenerate system in which a mean free path (L) can be defined:

$$S = \pm \frac{k}{e} \left(\frac{\Delta E}{kt} + A \right) \tag{18}$$

where $\Delta E = E_F - E_V$, is the energy difference between the Fermi-energy and the band edge in which conduction is taking place, i.e. conduction or valence band, and as mentioned above, is temperature dependent, e.g. equation 15. The constant A may take on various values depending on the energy dependence of the charge-carrier relaxation time, e.g. A = 2 for acoustical-mode lattice scattering[21]. If a mean free path cannot be defined, i.e. L < the lattice spacing, and the energy dependence of the density of states (and, hence, the conductivity) is assumed to be linear then A = (1 + terms of order T).

For a two carrier system the individual contributions of electrons (e) and holes (h) to the Seebeck coefficient are subtractive[22]:

$$S = \frac{\sigma_e S_e + \sigma_h S_h}{\sigma_e + \sigma_h} \tag{19}$$

In the experimental arrangement a Pt wire and a chromel-constantan thermocouple were pressed into contact with two of the platinum electrodes on the substrate using teflon-discs attached to phosphor-bronze strips (fig. 6). A Keithley 604 differential voltmeter was connected to the platinum leads to measure the Seebeck voltage across the film and then to the two thermocouples, connected differentially, to measure the temperature gradiant. A temperature gradiant of $\sim$5°C., near room-temperature, was established in the films perpendicular to the platinum electrodes by placing the substrate on a half-copper, half-teflon heat-sink (fig. 6) and heating the copper by a hot-plate. In a separate experiment a Pb film was evaporated onto a Pt-electroded substrate and the absolute Seebeck coefficient of the electrodes was determined to be $\sim$2μV/°C with Pt leads and +2μV/°C with constantan leads.

Values of S for various films are plotted against composition in fig. 7. All values were positive showing the majority carriers to be holes. Since for most films there was no evidence of impurity or defect band conductivity either from the temperature dependence of the conductivity or from the magnitude of σ_o equation 17 was rejected. Values for ΔE obtained from equation 18, for any reasonable assumed value for A, could not be reconciled with the ΔE values obtained from lnσ versus 1/T curves. We were, therefore, forced to conclude that equation 19 is applicable i.e. that the Fermi level is fixed near the middle of the energy gap and that both holes and electrons are contributing to the Seebeck coefficient.

7. Discussion

Attention has been drawn to the importance of annealing or depositing amorphous films near the crystallization temperature, T_c, to obtain reliable optical and conductivity data[23,24,25] Sb-Se films cannot be annealed because of the tendency to crystallize. Amorphous Sb films, of thickness $> 10^3 Å$, crystallize well below room temperature and amorphous Se crystallizes at $\sim 100°C$. The highest T_c reported for this system was 170°C at the composition Sb_2Se_3[26]. Because of the slow deposition rates ($\sim 2Å/sec$), the high vacuum ($\sim 10^{-7}$ mm Hg), and the proximity of the substrate temperature during deposition to T_c, it was thought unlikely that further annealing would produce changes in film structure.

From straight-line slopes of the $\ln\sigma$ versus $1/T$ curves it is evident that the Fermi-level is pinned in the gap. We cannot say whether this is due to a high local density of defect states in the gap as envisaged by Davis and Mott[27] or by a charge neutrality condition involving localized states tailing into the gap and overlapping, i.e. the CFO model[28]. Unfortunately, in our case, the Fermi-energy could not be determined by thermo-emf measurements; the low Seebeck coefficient values clearly indicate that we are in a two-carrier mode of conduction.

A comparison between the optical (E_g) and thermal (ΔE) activation energies as a function of composition is shown in fig. 8. A break in both curves occurs in the vicinity of Sb_2Se_3. At this composition $2\Delta E \simeq E_g$ from which we might infer a symmetrical distribution of states with the Fermi-level pinned near the center of the gap. Since ΔE strictly represents the difference between the Fermi-level and the valence-band edge, no great importance should be attached to the fact that $2\Delta E > E_g$ at high

Sb concentrations or $< E_g$ at high Se concentrations. One cannot justifiably assume that the difference between $2\Delta E$ and E_g represents the energy spread of the localized levels at the band edge as supposed by Weiser and Brodsky[29] for amorphous As_2Te_3 (where $2\Delta E > E_g$) or by Chandhari et. al.[15] for amorphous $3As_2Se_3 \cdot 2Sb_2Se_3$ films (where $2\Delta E > E_g$). Possible reasons for this difference are:

i) the Fermi-level may be fixed away from the middle of the gap either by a high density of defect (or impurity) states[27] or by a different energy distribution of localized states tailing into the gap[28];

ii) the value of ΔE obtained from the $\ln\sigma$ versus $(1/T)$ curves represents the extrapolated value to absolute zero assuming a linear variation (constant γ) of ΔE with temperature, which is not generally equal to the true value of ΔE at absolute zero[12,18];

iii) the optical energy gap is difficult to define since the lower part of the absorption edge is generally exponential with $h\nu$ and of uncertain origin[12] (does not obey Urbach's rule) and, at higher photon energies, obeys a power law of the form $\alpha h\nu \propto (h\nu - E_g)^n$ where $0.5 \leqslant n \leqslant 3$, which, depending on the assumptions used in the derivation, will give a different meaning to the value of E_g as determined by extrapolation;

iv) the variation of the optical gap E_g is generally assumed linear down to absolute zero for comparison with ΔE, which is rarely the case;

v) the demarcation between localized and non-localized states at the band edges is not clearly defined and depends to some extent on the localized state's distribution in energy[12].

Values of $\sigma_0 \exp(\frac{\gamma}{k}) \sim 10^3$ ohm^{-1}cm^{-1} are found for compositions on the Sb-rich side of Sb$_2$Se$_3$. On the Se-rich side the values steadily decrease to ~ 10 ohm^{-1}cm^{-1}. Assuming an average value of 60 for $\exp(\frac{\gamma}{k})$ (i.e. the value obtained for amorphous Sb$_2$Se$_3$ between 200°K and 300°K)[30] for all compositions then the magnitude of σ_0 suggests conduction in extended states for the Sb-rich films and conduction in localized states at the band edges for the Se-rich films.

The optical data showed an expected increase in the high (ε_∞) and low frequency (ε_0) dielectric constants, with increasing Sb (metallic-bonding) content. Absorption coefficients (α) ranged from 10^3 to 10^5 cm^{-1} for the particular experimental conditions (film-thickness, spectrometer sensitivity, etc.) and fitted well to an $(\alpha h\nu)^{\frac{1}{2}}$ versus $h\nu$ relationship for non-direct transitions showing the k-conservation selection rule is relaxed. An exponential tail was not observed or expected for these high absorption constants. The slope (B) of the curves showed a steady increase with increasing Se-content.

Davis and Mott[27] have shown that B can be related to the energy spread (ΔE_1) in localized states at the band edge by

$$B = \frac{4\pi\sigma_0}{nc\Delta E_1} \tag{20}$$

where it is assumed that the optical transitions are occuring between extended and the localized states and that $\sigma_{opt} \sim \sigma_0$. Table 1 lists the values of ΔE_1 calculated from the slopes assuming $\exp(\frac{\gamma}{k}) = 60$. It can be seen that the values are very small $\sim 10^{-2}$ to 10^{-4}eV and tend to decrease with increasing Se-content. However, when σ_0 drops much below a value $\sim 10^2$ ohm^{-1}cm^{-1}, it can no longer be assumed to be $\sim \sigma_{opt}$ and equation 20 cannot be used to determine a value of ΔE_1. We can only infer

from the small values of σ_0 that conduction occurs by hopping in localized states and, hence, that ΔE_1 must increase at high Se content. A second difficulty arises, namely, that even in the range of high σ_0 the values obtained for ΔE_1 are very much smaller than the photon energy range (> several tenths eV) over which equation 9 applies.

We are forced to conclude that the assumption of parabolic bands used by Tauc[13] in the derivation of equation 9 is more applicable to our films, that there is no evidence of appreciable band tailing, i.e. the band edges are fairly sharp, and the low values of σ_0 at high Se concentrations are the result of a low diffusion-type mobility in extended states rather than hopping in localized states. Cohen[19] has estimated that this Brownian-motion conductivity extends from $\sim$ 5 $cm^2/$volt sec down to 10^{-2} $cm^2/$volt sec., which coupled with the increasing gap with Se-content would well encompass the range of conductivities encountered in our films.

Further support for these conclusions is given by a comparison of conduction in amorphous Sb_2Se_3 and conduction in a single crystal of intrinsic Sb_2Se_3[31]. Between 300°K and 100°K, the conductivity in the c-direction of the single crystal was characterized by an activation energy of 0.63 eV with $\sigma_0 \sim$ 33 $ohm^{-1}cm^{-1}$ and σ (room-temp.) $\sim$ 5 x 10^{-8} $ohm^{-1}cm^{-1}$. This compares with the amorphous film of Sb_2Se_3, which has an activation energy of 0.625 eV, $\sigma_0 \sim$ 12 $ohm^{-1}cm^{-1}$ and σ (room-temp.) $\sim$ 2 x 10^{-8} $ohm^{-1}cm^{-1}$ and shows that the mobility is comparable in both phases. Black et. al.[32] estimated the hole mobility in crystalline Sb_2Se_3 to be approximately 45 $(m_0^2/m_e m_h)^{3/4}$. Optical absorption[33] and photoconductive spectral response[34] measurements on single crystal and amorphous Sb_2Se_3 show almost identical values for the energy gap; again showing the properties of the two phases are remarkably similar[35].

The continuous change in energy gap and conductivity with composition lends support to the view that foreign atoms incorporated in an amorphous solid tend to satisfy their valency requirements rather than act as donor or acceptor impurities. Sb, when added to amorphous Se, probably reduces the Se_8 ring concentration (as with As)[35] and acts as a branching or cross-linking agent between the Se linear polymer chains, replacing the weak bonds between chains with stronger covalent bonds. The fact that the addition of Sb reduces the glass-forming capability of Se[37] from the melt is more related to modification of the coordination (it becoming more metallic) in the melt than to cross-linking in the solid. Amorphous Sb_2Se_3 has a higher crystallization temperature than amorphous Se.

The following hypothesis based on a chemical bonding model is advanced to account for the tremendous variation of energy gap with composition. The valence band in undoped amorphous Se is assumed to arise from the non-bonding (lone-pair) 4p states and the conduction band from anti-bonding σ^* states arising from p orbitals[38]. From the relative energy positions of the molecular states of Sb and Se, the addition of Sb to Se would provide unoccupied Sb σ^* (anti-bonding) states just below the Se σ^* conduction band and Sb σ (bonding) states below the Se (non-bonding or lone-pair) valence band[39]. However, Sb-Se bonds will be formed which will probably be of the resonating p-type. At low concentrations of Sb, these bonds will create localized σ^* states below the Se σ^* band. At higher concentrations of Sb the states will become delocalized and form the conduction band and, in addition, the valence band will probably take on a resonating p-state character, first producing localized and then delocalized states, as the composition Sb_2Se_3 is ap-

proached. The general overlap of the states and the consequent broadening of the bands would account for the decrease of optical activation energy between pure Se and Sb_2Se_3. A further increase in Sb concentration would result in its domination of the band structure, and particularly the interaction of the Sb 5d orbitals, which at very high Sb concentrations would produce appreciable overlap into the energy gap. Near pure Sb, these orbitals would be depressed into the valence band, causing the conductivity to be metallic upon crystallization.

An added reason for the decrease in bandgap with Sb concentration could be due to the effect of compositional disorder[39]. Lone-pair electrons adjacent to Sb atoms will have higher energies than those remote from Sb atoms, causing a broadening and tailing of the lone-pair valence band of Se. This effect could account for the shallower slope of the $(\alpha h\nu)^{\frac{1}{2}}$ versus $h\nu$ curves with increasing Sb concentration.

We wish to thank Dr. J.C. Shaffer for valuable discussions and comments on this work.

References

1) R. Mueller and C. Wood, J. Non-Crystalline Solids 7 (1972) 301.

2) S.A. Vikshinsky, New Method of Metallographic Analysis of Alloys Gov. tekch. izdat, 1944.

3) M.V. Kot and I.P. Molodyan, Uchenye Zapiski Kishinev Univ. 39 (1959) 49.

4) W.J. Ostrander and C.W. Lewis, Trans. Natl. Vacuum Symp. 8 (1961) 881.

5) These equations are essentially the same as in Ref. 4 but expressed in terms of atomic weights.

6) H.R. Smith, Society of Vacuum Coaters Annual Meeting, Detroit Mich. March 5-6 (1969).

7) L.S. Palatnik and V.M. Kosevich, Soviet Phys. Cryst. $\underline{3}$ (1958) 716.

8) J. Cohen, J. Appl. Phys. $\underline{25}$ (1954) 798.

9) J. Strong, Procedures in Experimental Physics (Prentice-Hall, N.J. 1938) p. 376.

10) T.M. Donovan, W.E. Spicer, J.M. Bennett and E.J. Ashley, Phys. Rev. $\underline{2}$ (1970) 397.

11) H.E. Bennett and J.M. Bennett, Physics of Thin Films (ed. G. Haas and R.E. Thun) $\underline{4}$ (Academic Press, N.Y. 1967) 31.

12) E. Davis and N.F. Mott, Electronic Processes in Non-Crystalline Materials (Clarendon, Oxford, 1971).

13) J. Tauc, Optical Properties of Solids (ed. F. Abèles) (North-Holland, Amsterdam, 1970).

14) T.S. Moss, Optical Properties of Semiconductors (Butterworths, London, 1961).

15) P.K. Chandhari, E.R. Chenette and A. Van Der Ziel, J. Appl. Phys. $\underline{43}$ (1972) 3145.

16) F. Abèles, Ann. d. Phys. $\underline{5}$ (1950) 596, ibid 706.

17) J.S. Blakemore, Electrical Communication, (June, 1952) 131.

18) H. Fritzsche, J. Non-Cryst. Solids $\underline{6}$ (1971) 49.

19) M.H. Cohen, J. Non-Cryst. Solids $\underline{4}$ 391 (1970).

20) A. Lewis, Phys. Rev. Lett. $\underline{29}$ (1972) 1555.

21) A.F. Joffe, Semiconductor Thermoelements (Infosearch, London, 1957).

22) V.A. Johnson, Progress in Semiconductors $\underline{1}$ (1956) 82.

23) W.E. Spicer, T.M. Donovan and J.E. Fischer, J. Non-Cryst. Solids $\underline{8-10}$ (1972) 122.

24) M.L. Theye, Mat. Res. Bull. $\underline{6}$ (1971) 103.

25) P.A. Walley and A.K. Jonscher, Thin Solid Films, $\underline{1}$ (1967) 367, ibid, $\underline{2}$ (1968) 327.

26) L.R. Gilbert and C. Wood, Bull. Am. Phys. Soc. $\underline{16}$ (1971) 500.

27) E.A. Davis and N.F. Mott, Phil. Mag. $\underline{22}$ (1970) 903.

28) M.H. Cohen, H. Fritzsche and S.R. Ovshinsky, Phys. Rev. Lett. $\underline{22}$ (1969) 1065.

29) K. Weiser and M.H. Brodsky, Phys. Rev., $\underline{1}$ (1970) 791.

30) B. Van Pelt and C. Wood (to be published).

31) L.R. Gilbert and C. Wood (to be published).

32) J. Black, E.M. Conwell, L. Seigle and C.W. Spencer, J. Phys. Chem. Solids $\underline{2}$ (1957) 240.

33) C. Wood, Z. Hurych and J.C. Shaffer, J. Non-Cryst. Solids $\underline{8-10}$ (1972) 209.

34) Z. Hurych, R. Mueller, C.C. Wang and C. Wood, J. Non-Cryst. Solids $\underline{11}$ (1972) 153.

35) Switching has also been observed in both amorphous and crystalline phases of Sb_2Se_3 c.f. S. Luby, J. Cervenak, J. Kubek, M. Marcin and J. Schilder, Czech. J. Phys. B$\underline{21}$, 878 (1971) and L.G. Gribnyak, Sov. Phys.-Semicond. $\underline{6}$ 478 (1972).

36) G. Lucovsky, Mater. Res. Bull. $\underline{4}$ (1969) 505.

37) R.W. Haisty and H. Krebs, J. Non-Cryst. Solids $\underline{1}$ (1969) 399.

38) E. Mooser and W.B. Pearson, Progress in Semiconductors $\underline{5}$ (1960) 103.

39) M. Kastner, Phys. Rev. Lett. $\underline{28}$ (1972) 355.

Table 1

Optical and electrical parameters of amorphous
Sb-Se films as a function of composition

Film #	At % Se	E_g(eV)	B(cm^{-1}eV^{-1}) x 10^5	ΔE(eV)	$\sigma_o \exp(\gamma/k)$ (ohm^{-1}cm^{-1}) x 10^3	ΔE_1(eV)
L2	11.5			1.6×10^{-4}	28.9	
L4	15			.255	1.37	
L5	17.5	.40	2.7			1.37×10^{-2}
L6	21			.308	3.45	
L7	24.5	.51	3.4			1.07×10^{-2}
L8	29			.347	1.97	
L9	30.5	.72	3.7			9.44×10^{-3}
L10	41			.458	1.25	
L11	48	.95	3.8			8.98×10^{-3}
L12	55			.591	1.08	
L13	60	1.41	7.0			9.43×10^{-4}
L14	69			.656	0.12	
L15	75	1.55	7.8			1.36×10^{-4}
L16	80			.674	.0017	
L17	84	1.68	9.2			
L19	90	1.77				
L25	97	1.89	10			
U3	50	1.00	5.0			
U7	56.5	1.16	6.5			
U10	62			.647	.54	
U12	65			.649	.32	
U13	67	1.33				
U19	76	1.54				
U27	84	1.63	7.1			

Table 2

High (ε_∞) and low (ε_0) frequency dielectric constants
obtained from extrapolation of curves in fig. 4

Sample	ε_0	ε_∞
L25	5.8	12.3
L19	7.2	13.75
L13	12.8	33.5
L7	20.7	54.0

Figure Captions

Fig. 1.   Coevaporation system.

Fig. 2.   Theoretical curves of composition (C) and film thickness (T) versus film position in upper (U) and lower (L) substrate holders. x - μ-probe data, o - thicknesses determined by interferometry.

Fig. 3.   Square-root dependence of absorption coefficient (α) on photon energy (hν) for Sb-Se films of varying compositions shown in fig. 2.

Fig. 4.   Square of the refractive index (n) determined from interference maxima and minima and from equation 7 versus square of wavelength (λ). Theoretical points: o - interference, x - cubic equation.

Fig. 5.   Electrical conductivity (σ) versus reciprocal of absolute temperature (T).

Fig. 6.   Diagram of electroded substrate showing spring contacts for thermo-emf measurements. 4 spring contacts, without teflon discs, were used for electrical conductivity measurements.
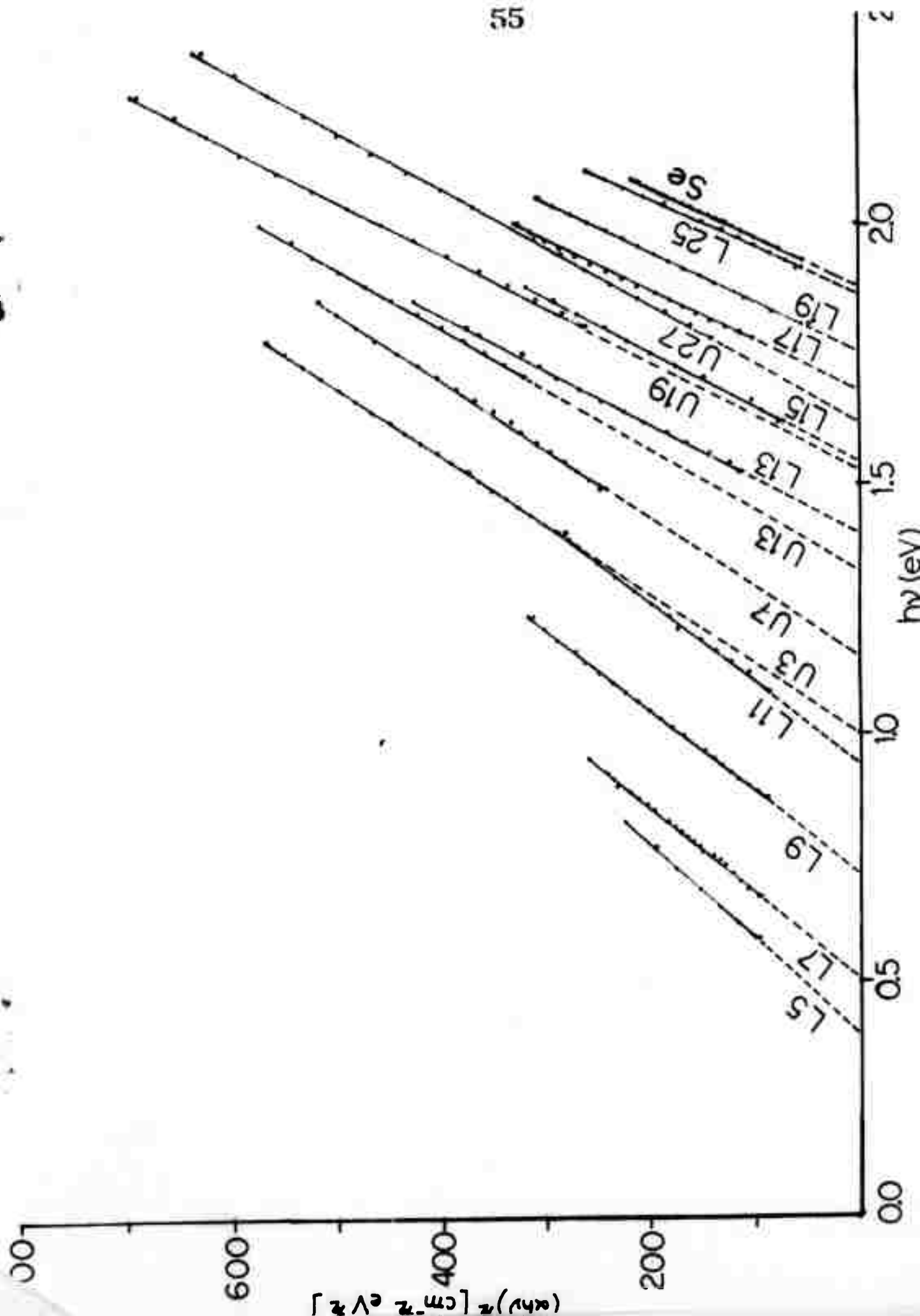
Fig. 7.   Seebeck coefficient versus film composition.

Fig. 8.   Optical (o) and thermal (x) activation energies as a function of film composition.
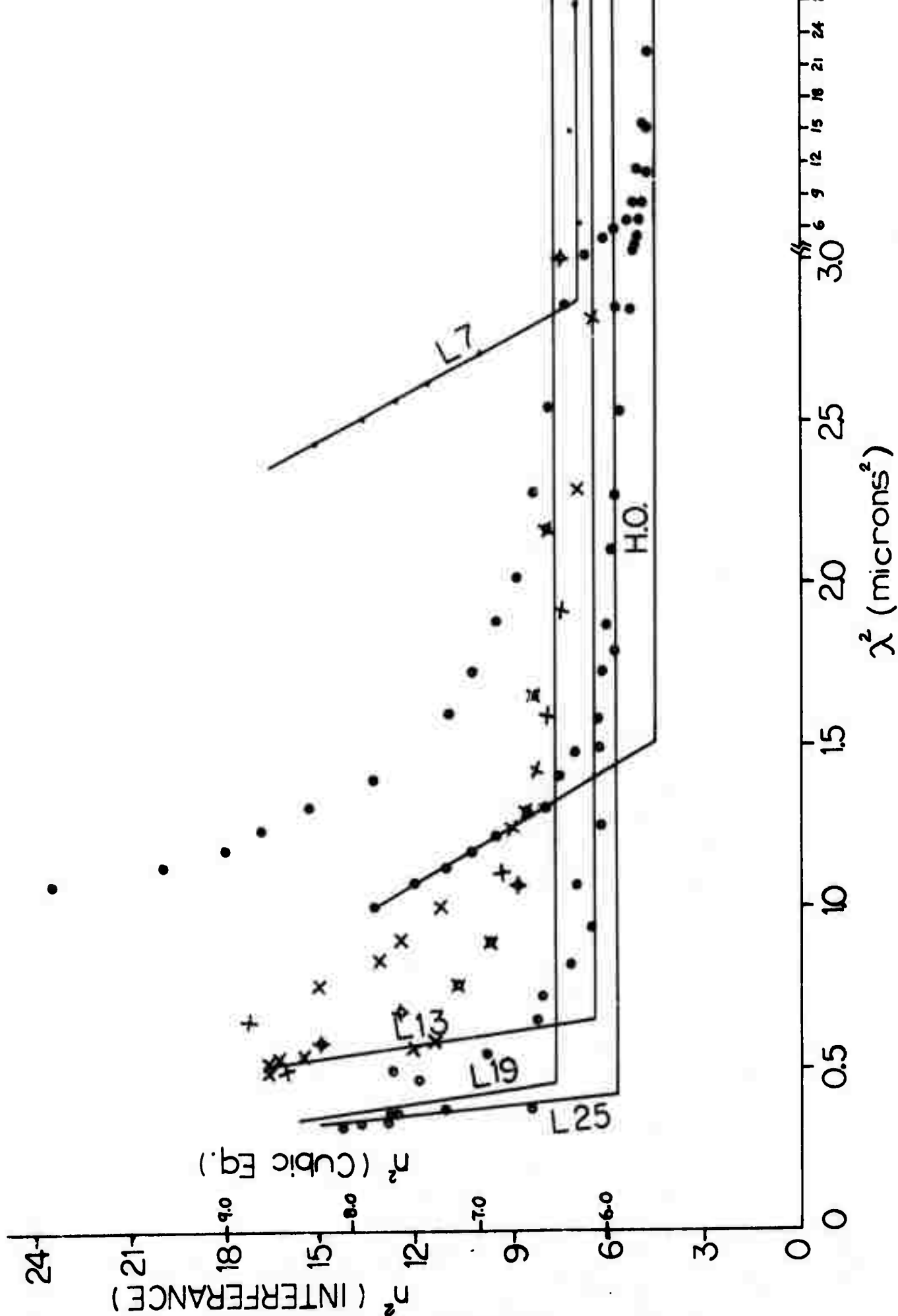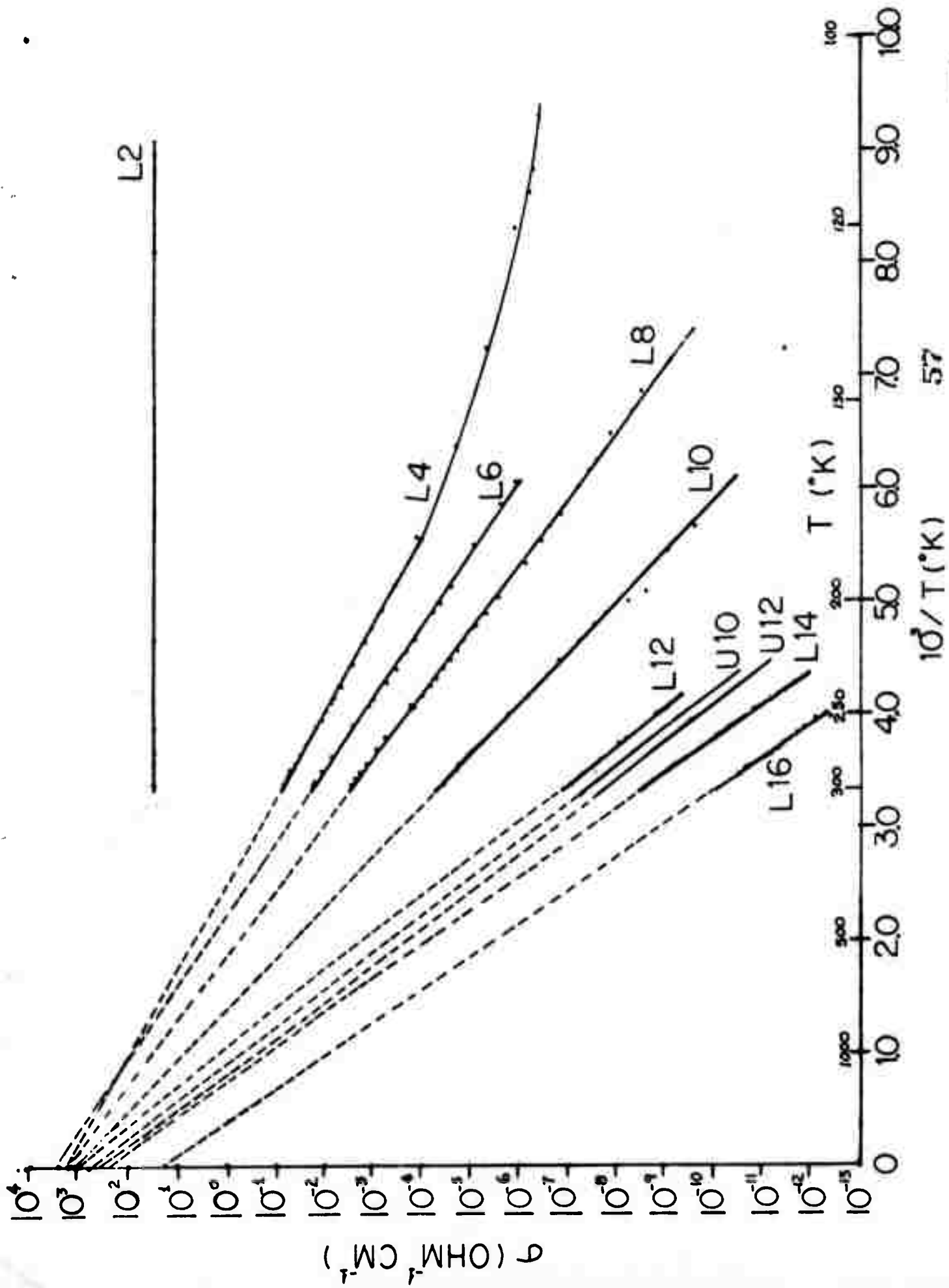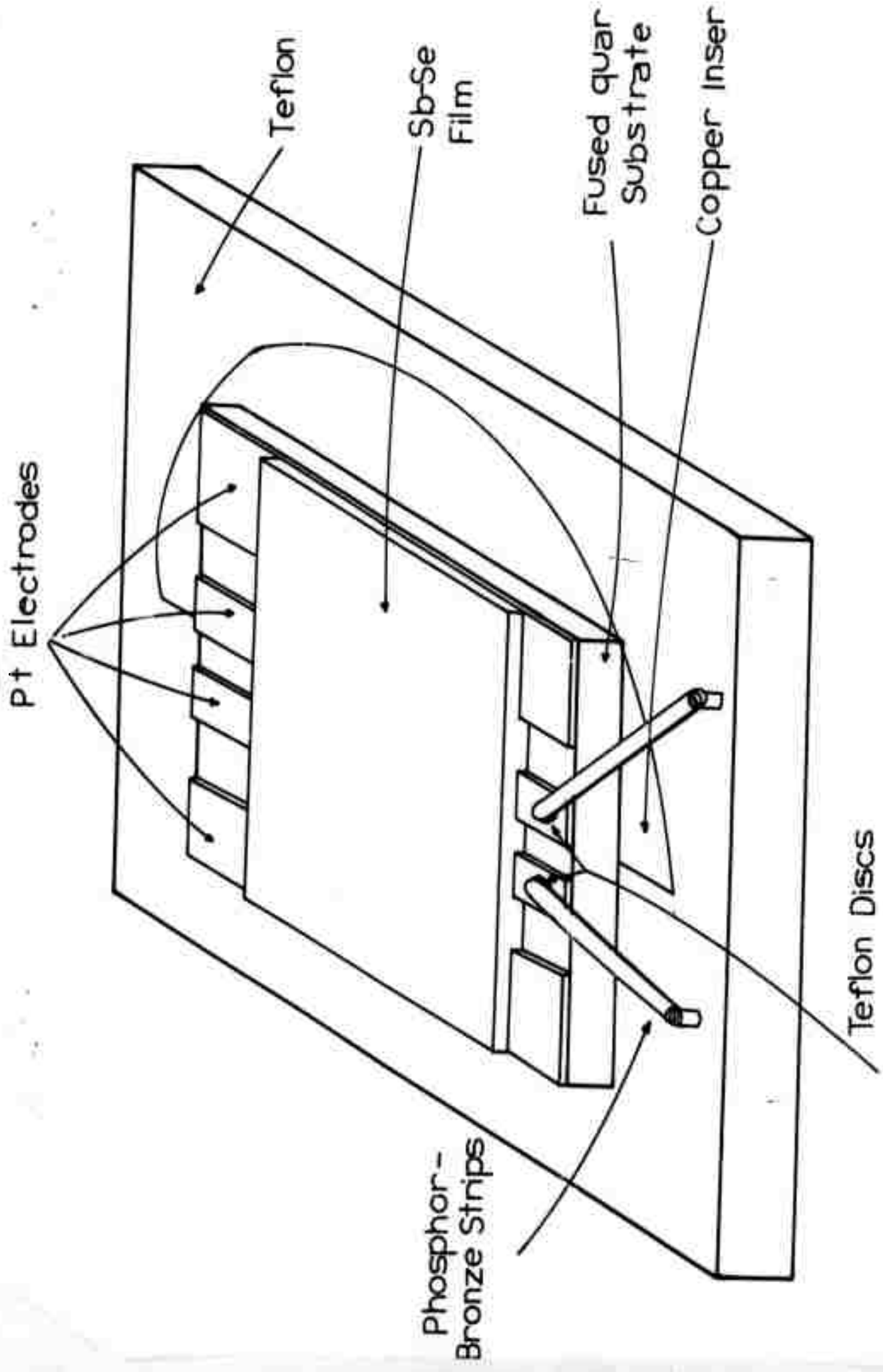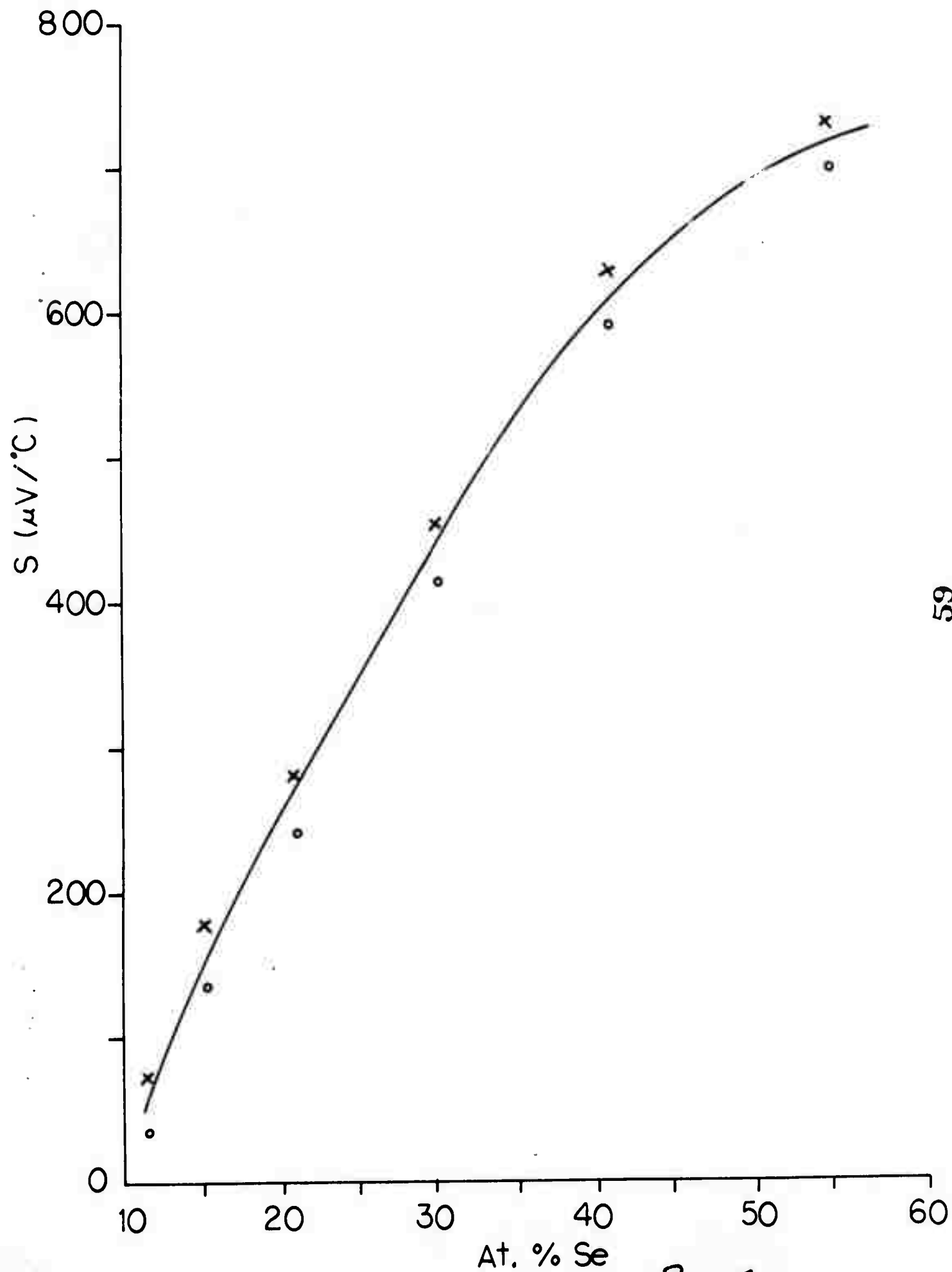
FIGURE 1: COEVAPORATION SYSTEM

Fig 2.4

54

Se

L25

L9

L17

U27

U15

U19

L13

U11

U7

U3

L11

L9

L7

L5

$(\alpha h\nu)^{1/2} \left[cm^{-1/2} \ eV^{1/2} \right]$

$h\nu \ (eV)$

0.0   0.5   1.0   1.5   2.0

200   400   600   00

FIG. 4110

λ^2 (microns^2)

n^2 (INTERFERANCE)

n^2 (Cubic Eq.)

L7

L13

L19

L25

H.O.

FIG 5 W/O

σ (OHM^{-1} CM^{-1})

$10^3/T$ (°K)

T (°K)

L2

L4

L6

L8

L10

L12

U10

U12

L14

L16

Teflon

Sb-Se Film

Fused quar Substrate

Copper Inser
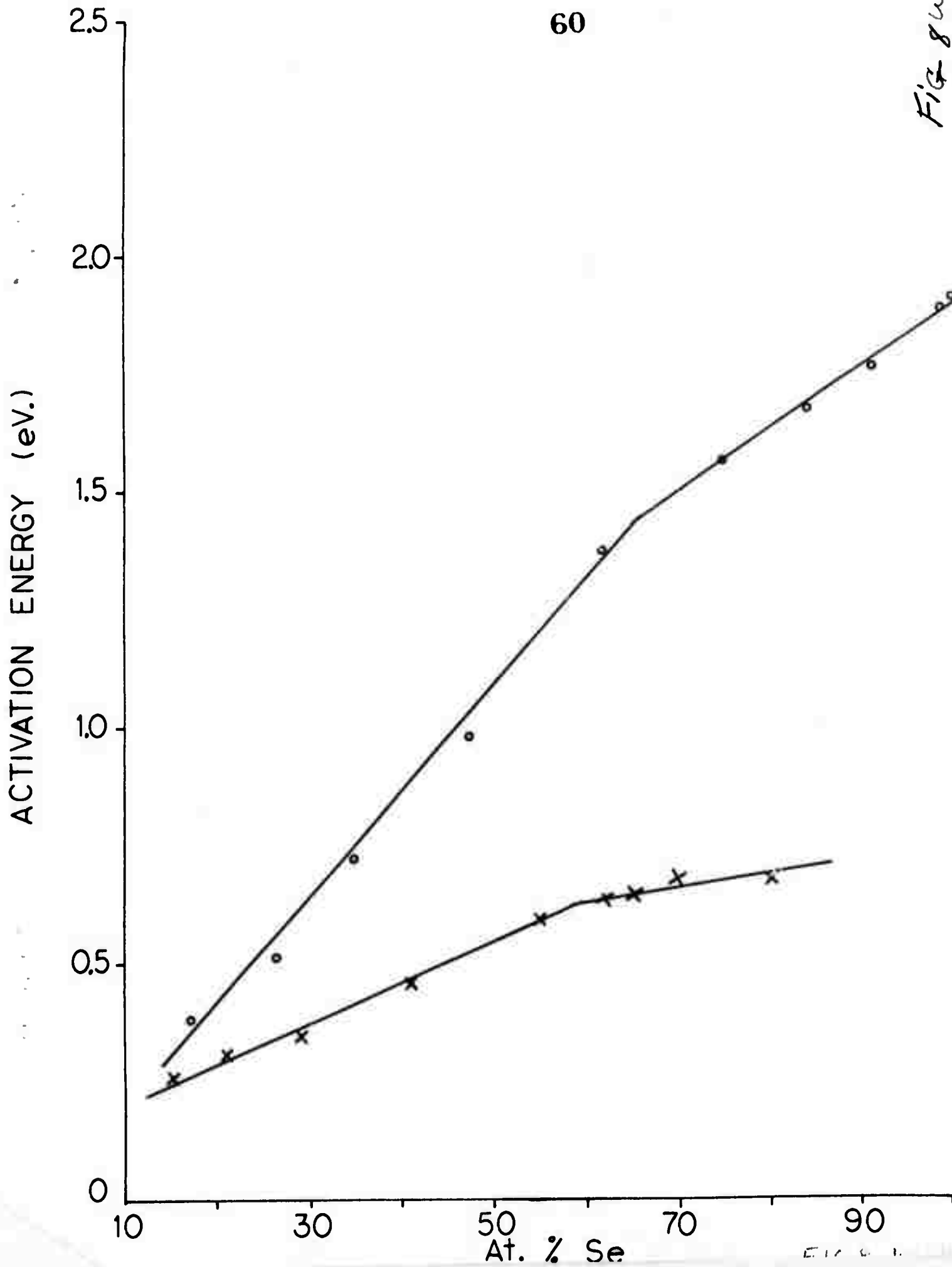
Pt Electrodes

Phosphor- Bronze Strips

Teflon Discs

FIG 6

58

fig 7

Fig 8 w
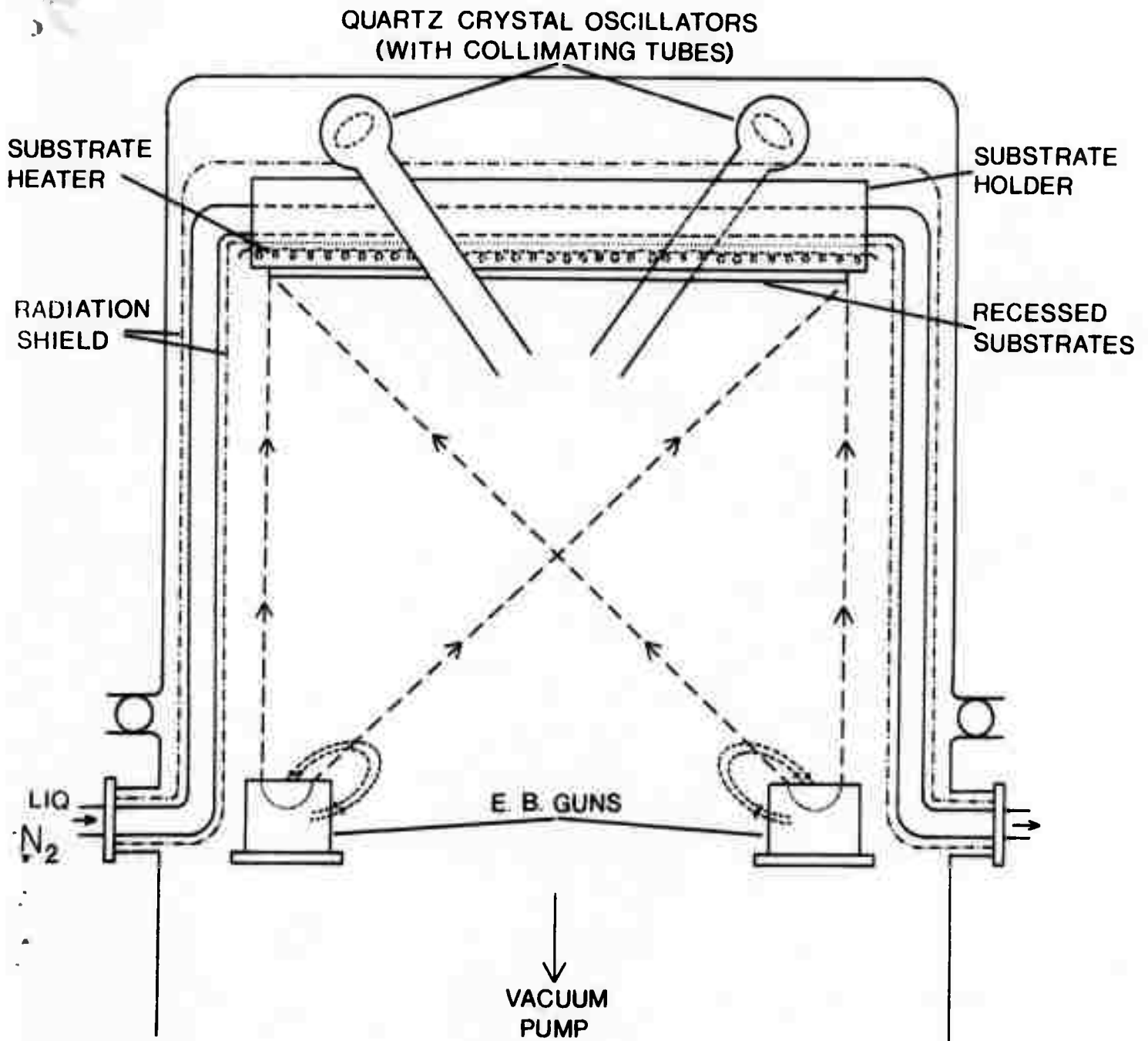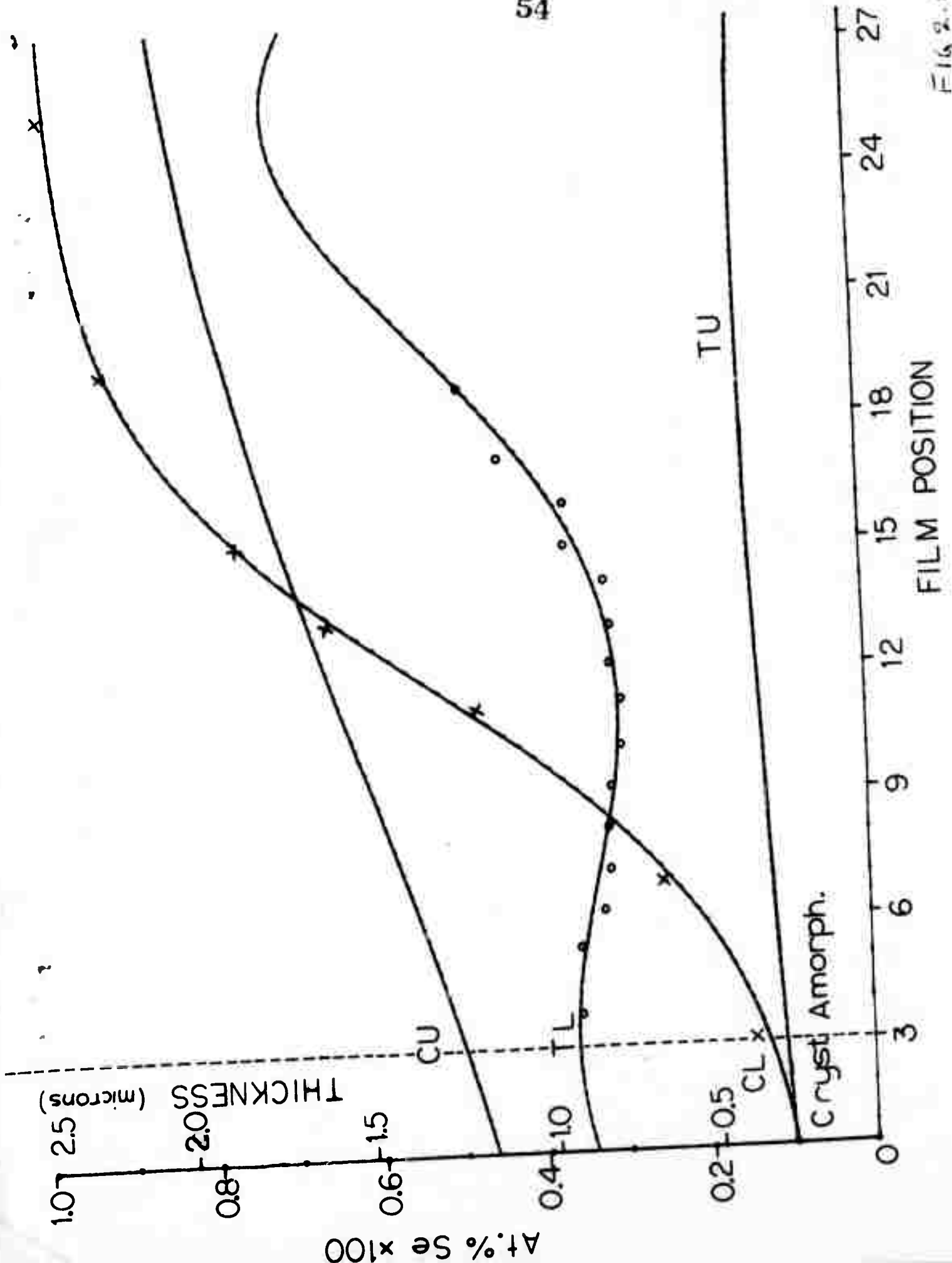
APPENDIX C

PHOTOCONDUCTIVITY IN Sb_2O_3.*

B. Wolfing and Z. Hurych

Physics Department
Northern Illinois University
DeKalb, Illinois 60115

Photoconductivity measurements were performed on crystals of cubic and orthorhombic antimony oxide (Sb_2O_3). Crystals were prepared using the vapor transport method from 6-9's purity elements as described in (1). Orthorhombic needles with growth axis in the c-direction were formed in a fused-quartz tube in the region just above 570° C. Triangular faceted cubic crystals were formed in the region just below 570° C. In addition, material in the form of an amorphous film was deposited on the walls of the tube. Silver paste was used to provide electrical contacts. The contacts were carefully shielded from illumination to avoid any photovoltaic effects. The samples were exposed to monochromatic light from a high intensity Baush-Lomb monochromator with a xenon source, chopped mechanically at a frequency of 37 c.p.s. The a.c. photoconductivity was measured with a Keithley 82 series lock-in amplifier.

Due to the small sample size, a quartz light pipe was used to direct the light beam to the sample. To obtain a normalized photoresponse, the monochromator light intensity was measured in the U.V. region using a sodium salicylate coated EMI photomultiplier. Sodium salicylate is known to

possess constant fluorescent quantum efficiency for λ<3400Å [2], [3]. Thus the monochromator output flux could be measured with great accuracy in the region of interest. For the orthorhombic crystals a sheet polarizer was used to polarize the light parallel to the c and b axes.

For both polarization directions of orthorhombic Sb_2O_3 the photoconductivity onset occurs at about 3.17 eV. Using the Moss' criterion [4] for the half-maximum photoresponse, we obtain an activation energy of 3.25 eV for $\vec{E}||b$, and 3.29 eV for $\vec{E}||c$. These values are in excellent agreement with the indirect energy gap values obtained in [1] which are 3.25 eV and 3.30 eV, respectively.

In the case of cubic Sb_2O_3 the photoconductivity onset occurs at about 3.10 eV. Fig. [3] shows an extrinsic photoresponse peak coinciding with the small peak in the optical absorption coefficient data, occuring at energies below the band gap. Such absorption can be due to crystal impurities or to native lattice defects, (this absorption does not show up in the orthorhombic Sb_2O_3 grown from the same melt and probably arises from defects). Therefore no attempt was made to use the Moss criterion since it is only applicable to inter-band transitions. Since the extrinsic optical absorption results in a photoconductive process we conclude that this process results in creation of free carriers rather than of excitons, unless the latter immediately dissociate. Contrary to expectations, in the short wave length region Fig. [3] we see that the photoresponse drops off sharply while the absorption coefficient is rising steadily, indicative of an onset of inter-band transitions. Most likely the sharp drop in photoresponse is due to strong surface recombination in the higher photon energy region.
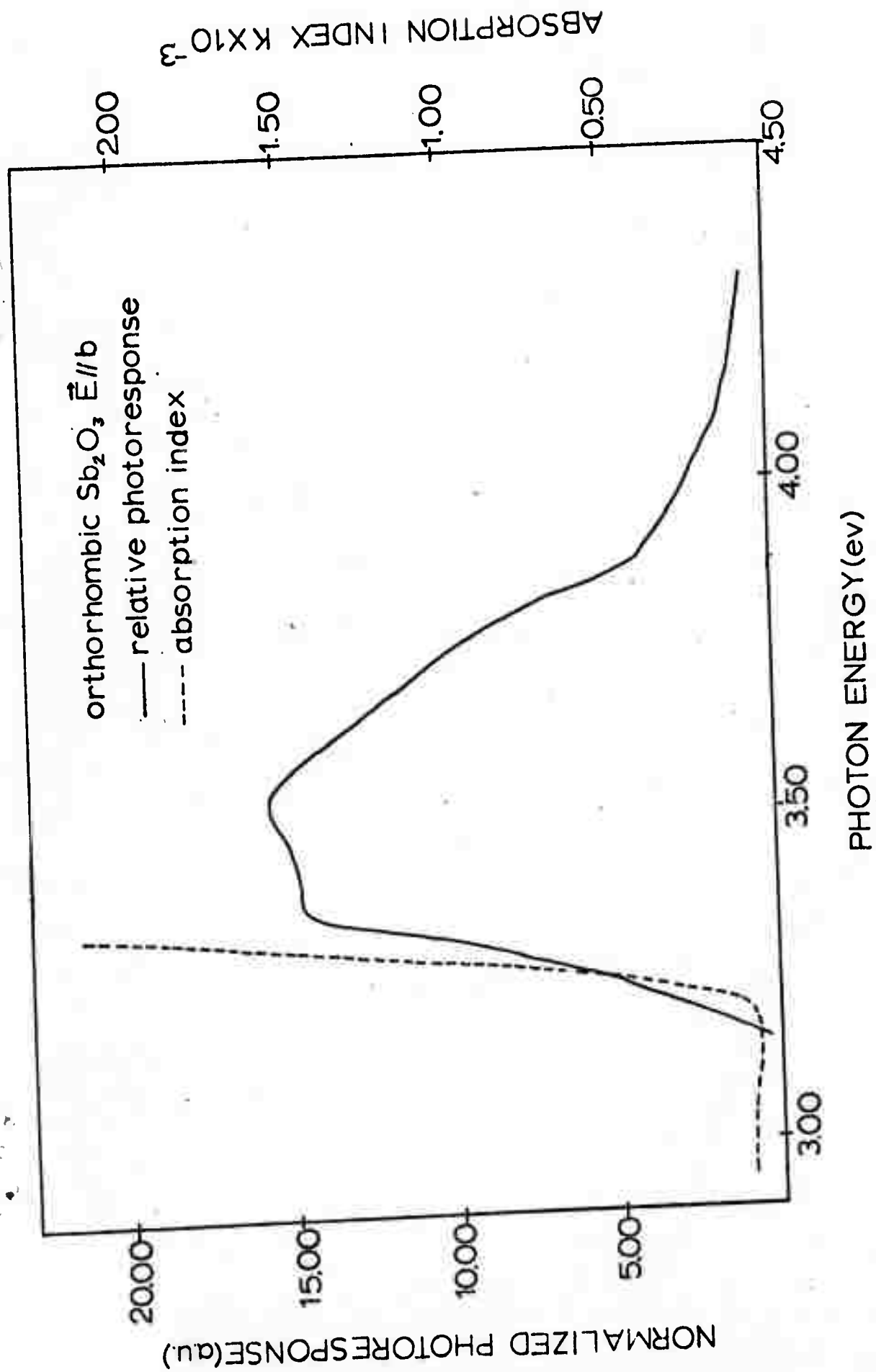
Many attempts were made to measure the photoconductivity of amorphous Sb_2O_3. All attempts failed. These results were not unexpected, since the photosensitivity of the amorphous phase could be several orders of magnitude less than that of the crystalline phase. In this regard it should be noted that even in the cubic crystal we were unable to measure the photoresponse in the intrinsic absorption region, due probably to strong surface recombination.
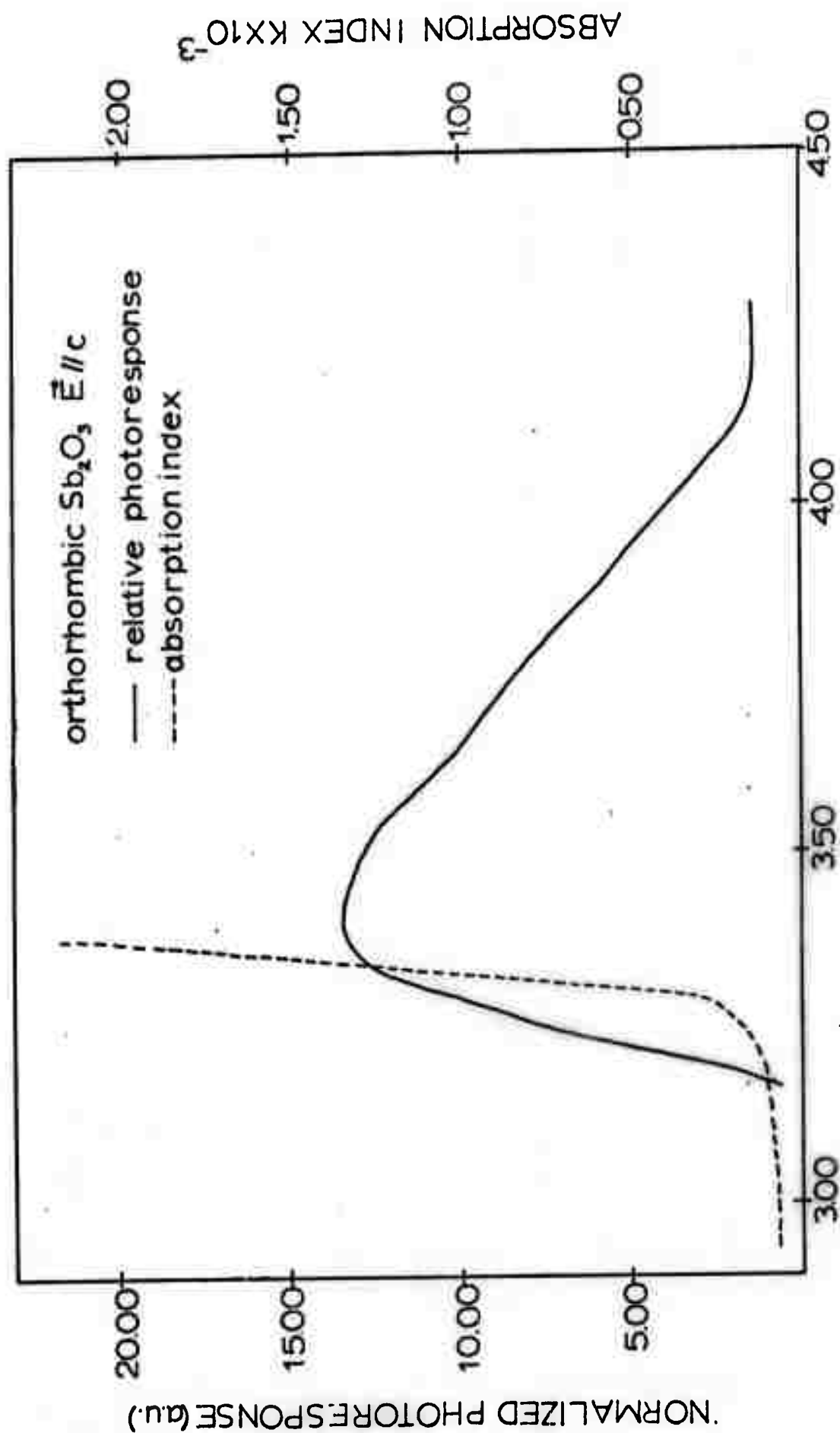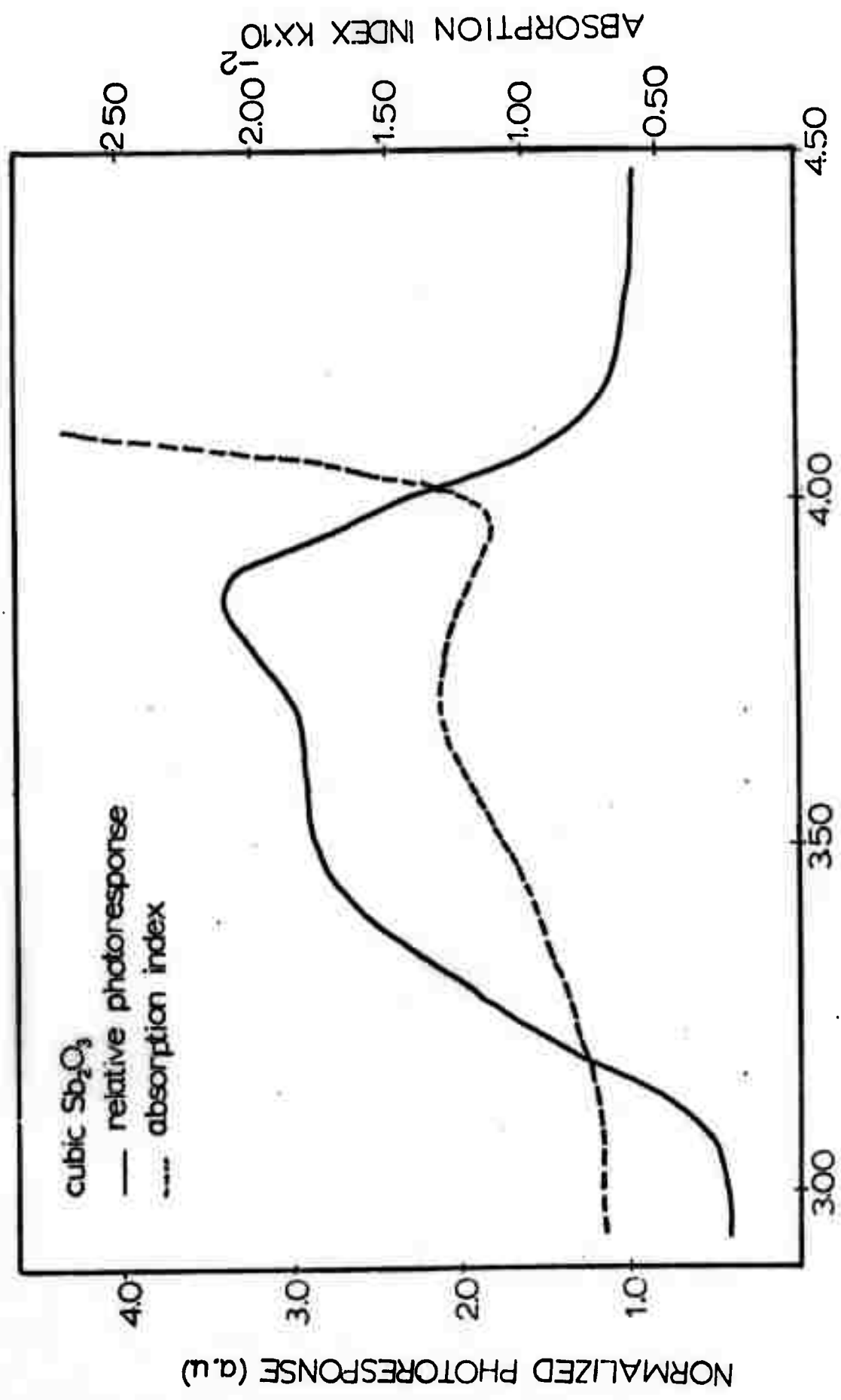
1. C. Wood, B. Van Pelt, A. Dwight, phys. stat. sol.

2. F.S. Johnson, K. Watanabe, R. Tousey, J. Opt. Soc. Am. 41, 702 (1951)

3. J. Hammann, Z. Agnew, Phys. 10, 187 (1958)

4. T.S. Moss, Photoconductivity in the Elements: (Academic press, N.Y. 1952)

5. Z. Hurych, R. Mueller, C.C. Wang, and C. Wood, J. Noncryst. Solids II, 153 (1972)

6. A. Rose, concepts in photoconductivity and allied problems; John Wiley and Sons, New York (1963)

Captions to Figures

Figs. 1, 2, 3: Normalized photoresponse, compared with the optical
absorption index, from ref 1, for orthorhombic ($E_0 || b$,
and $E_0 || c$) and cubic crystals of Sb_2O_3.

orthorhombic Sb_2O_3 $\vec{E}//b$

—— relative photoresponse
---- absorption index

ABSORPTION INDEX K×10³

NORMALIZED PHOTORESPONSE(a.u.)

PHOTON ENERGY(ev)

67

orthorhombic Sb_2O_3 $\vec{E}\,\|\,c$

— relative photoresponse
---- absorption index

ABSORPTION INDEX KX10⁻³

NORMALIZED PHOTORESPONSE (a.u.)

PHOTON ENERGY (ev)

68

cubic Sb_2O_3
— relative photoresponse
--- absorption index

ABSORPTION INDEX K×10⁻²

PHOTON ENERGY (ev)

NORMALIZED PHOTORESPONSE (a.u)

69

APPENDIX D

MOSSBAUER STUDY OF AMORPHOUS

SEMICONDUCTORS AND GLASSES

CONTAINING IRON, TIN AND ANTIMONY:

A Review*

S.P. Taneja and C.W. Kimball
Department of Physics
Northern Illinois University
DeKalb, Illinois 60115

Mössbauer Spectroscopy of Amorphous Semiconductors And Glasses Containing Iron, Tin and Antimony: A Review*

S.P. Taneja and C.W. Kimball
Physics Department
Northern Illinois University
DeKalb, Illinois 60115

A comprehensive review is given of Mössbauer studies, both experimental and theoretical, concerning the bond character, electronic structure and glass-crystal transition[1] in amorphous semiconductors and glasses[2] containing iron, tin and antimony. Plots of Mössbauer isomer shift vs. quadrupole splitting are given and interpreted in terms of electronic structure[3]. The isomer shift, in various tin and antimony containing systems, is correlated with electron density[4] (calculated from HFSCF) at the tin and antimony nuclei to delineate electronic structure in amorphous antimony chalcogenides[5,6] and alkaline-tin-silicate, alkaline-tin-borate glasses[7]. Similar calculations are made from the available data for many other amorphous systems; when possible, the Debye temperature is also computed. Comprehensive data on Mössbauer parameters will be presented along with a complete bibliography on the subject.

1) S.P. Taneja, A.E. Dwight, L. Gilbert, W. Harper, C.W. Kimball and C. Wood, Phys. Chem. Glasses, 13, No. 5 (Oct. 1972).

2) C.R. Kurkjian, J. of Non-Crystalline Solids 3, 157 (1970).

3) J.K. Lees and P.A. Flinn, J. Chem. Phys. 48 (2), 882 (1968).

4) S.L. Ruby, G.M. Kalvius, G.B. Beard and R.E. Snyder, Phys. Rev. 159, 239 (1967).

5) S.L. Ruby, L. Gilbert and C. Wood, Phys. Letters 37A, 453 (1971).

6) J.G. Stevens and L.H. Bowen in Mössbauer Effect Methodology, 5, (1969), p. 27.

7) K.P. Mitsofanov and T.A. Sidorov, Sovt. Phys.-Solid State, 9 (3) 693 (1967).